[UCI]I804:24011-200000334474

2020년 8월
석사학위 논문

폐쇄 루프 맥동 히트파이프의 열유동학적 특성에 대한 실험적 연구

조선대학교 대학원

기 계 공 학 과

히발 아흐마드

폐쇄 루프 맥동 히트파이프의 열유동학적 특성에 대한 실험적 연구

Experimental investigations on the thermo-hydrodynamic characteristics of closed-loop pulsating heat pipes (CLPHPs)

2020년 08월 28일

조선학교 대학원

기 계 공 학 과

히발 아흐마드

폐쇄 루프 맥동 히트파이프의 열유동학적 특성에 대한 실험적 연구

지도교수: 정성용

이 논문을 공학석사 학위신청 논문으로 제출함

2020년 05월

조선대학교 대학원

기 계 공 학 과

히발 아흐마드

히발 아흐마드의 석사학위 논문을 인준함

위원장 조선대학교 교수 박 정 수 ㊞
위 원 조선대학교 교수 조 홍 현 ㊞
위 원 조선대학교 교수 정 성 용 ㊞

2020년 6월

조선대학교 대학원

Contents

List of Figures

List of Tables

Nomenclature

FR	Filling ratio [%]
CLPHP	Closed Loop Pulsating Heat Pipe
LTF	Liquid Thin Film
PFV	Photron FASTCAM Viewer
PFA	Photron FASTCAM Analysis
DAQ	Data Acquisition
VP	Vapor Plug
LS	Liquid Slug
Nicr	Nickle-Chromium
CHF	Critical Heat Flux [W/cm^2]
FPS	Frame Per Seconds
L_{tot}	Total Length [mm]
mm	Millimeter [mm]
T_e	Evaporator Temperature [℃]
T_c	Condenser Temperature [℃]
T_{eavg}	Average evaporator temperature [℃]
T_{cavg}	Average Condenser Temperature [℃]
Q	Heat Load [W]
R_{th}	Thermal Resistance [℃/W]
V	Voltage [V]
I	Ampare [A]
K_{eff}	Effective thermal conductivity [W/m.K]

H_{eff}	Effective heat transfer coefficient [W/m.K]
ID	Inner diameter [mm]
OD	Outer diameter [mm]
V	Velocity [m/s]
G	Gravity [m/s^2]
q''	Heat Flux [W/cm^2]
A	Area [m^2]
ρ	Density [Kg/m^3]
σ	Surface tension [N/m]

Subscript

ax	Axial
rad	Radial
e	Evaporator
c	Condenser
l	Length
tot	Total
Eff	Efficient
v	Vapor
s	Slug
Bo	Bond Number
Crit	Critical

Abstract

Experimental investigations on the thermo-hydrodynamic characteristics of closed-loop pulsating heat pipes (CLPHPs)

Hibal Ahmad

Advisor: Prof. Sung Yong Jung, PhD.

Graduate School of Chosun University

Owing to the excess generation of heat in devices for applications such as electronic, space, and nuclear applications, it is essential to develop more economical, risk-free, and reliable thermal management devices. Material science, packaging concepts, fabrication technology, and novel cooling techniques are some key areas requiring research for successful thermal management. In recent decades, various two-phase passive cooling technologies based on latent heat transfer have been introduced, such as heat pipes, thermosyphons, vapor chambers, and loop heat pipes. The main advantages of these devices are their efficiency, adaptability, cost-effective nature, and passivity. Focusing on the two-phase heat transfer system, this thesis describes the complex thermo-hydrodynamic behaviors of the closed-loop pulsating heat pipes (CLPHPs), which is the new device in the family of two-phase passive heat transfer systems. Theses devices are very unique to their simple wickless structures. The performance of these devices is reliant on the internal bubble patterns which also defines the events and mechanisms, pressure, temperature, velocity, acceleration perturbations, flow regimes changes, bubbles displacements, etc. combining these factors also contributes to the thermal performance of the CLPHPs. The effect of the coolant source is also the major factor while

being neglected in previous studies. Considering the literature study, the heat transfer characteristics are varied for different devices and coolant sources, yet not fully understand and defined.

To understand the thermo-hydrodynamic of these two-phase heat transfer devices with checking its limits in different convection sources, two different experimental set-ups have been envisioned, fabricated and tested in a laboratory. The set-up is specially designed for flow visualization, which can better define the flow regime trends when the heat load is increased. The primary influence parameter which affects the thermo-fluidic properties of the systems are as follows;

- Convection source and length
- Volumetric filling ratio
- Fill ratio consistent with convection source
- Orientation
- Thermo-physical properties
- Heat flux

The thesis provides a detailed discussion on the performance of CLPHP when subjected to different convection sources under vertical bottom heating mode orientation, especially the limits were checked the convection sources in the first experiment. The optimal filling ratio was found out when the ambient conditioned cooled the system in another experiment. For two different experiments, two different working fluid is used, hence the performance has been checked with different thermo-physical properties. Of course, the flow regimes were captured for both of the experiments to understand the bubble dynamics with different convection sources and working fluid. Apart from the working fluid and heat flux, the

performance is strongly linked with the flow patterns existing inside the device. Delicate aspects of these two-phase flow dynamics and their relations with the heat transfer characteristics have been emphasized leading to the formulation of primary design rules. The present studies can be used as a scale for future innovative industrial applications based on its thermo-hydrodynamics properties.

Although some nuances of the device operation remain unexplored, it is believed that major advancement in the understanding of the thermo-hydrodynamics of CLPHPs for different convection sources, and the optimal filling ratio for natural convection has been accomplished.

한 글 요 약

폐쇄 루프 맥동 히트파이프의 열유동학적 특성에 대한 실험적 연구

히발 아흐마드

지도 교수: 정성용

대학원, 조선대학교

최근 전자, 우주 등의 응용분야에서 사용되는 장치에서는 과도한 열이 발생하기때문에 경제적이며 안정적인 열관리 장치의 개발에 대한 요구가 증가하고 있으며, 이를 위하여 재료, 생산 및 냉각 기술분야에서 관련연구가 활발하게 이루어지고 있다. 최근 수십 년동안, 고효율의 냉각 성능을 확보하기 위하여 히트 파이프(heat pipe), 써모싸이폰(thermosyphon), 증기 챔버(vapor chamber) 및 루프 히트 파이프(loop heat pipe)와 같은 잠열을 이용한 이상 (two-phase) 유동 수동 냉각 기술이 소개되고 있다. 본 논문에서는 이상 유동 수동 냉각 기술의 하나인 폐쇄 루프 맥동 히트파이프(closed-loop pulsating heat pipes, CLPHP)의 복잡한 열유동학적 거동에 대하여 연구하였다. 기존 히트 파이프와 비교할 때 CLPHP는 wick이 없는 단순한 구조로 그 성능이 우수하다고 알려져 있다. CLPHP의 성능은 내부 이상 유동 패턴과 밀접한 연관이 있으며, 내부 유동은 채널 크기, 채널 수, 냉각 장치 등 다양한 요인에 영향을 받는 것으로 알려져 있지만 아직까지 CLPHP 내부 유동에 대한 이해와 연구는 충분하지 않다. 본 논문에서는 다양한 요인 중에서 냉각이 CLPHP 내부 유동과 성능에 미치는 영향에 대하여 실험적 연구를 진행하였다.

냉각 장치가 CLPHP의 열유동학적 거동에 미치는 영향을 살펴보기 위하여 실험실 스케일에서 두 가지 다른 실험을 구성하고 실험을 진행하였다. 실험 장치는 유동가시화 기법을 적용하여 유동 패턴과 CLPHP 성능을 확인할 수 있도록 특별히 제작되었다. CLPHP의 열유동학적 특성에 미치는 주요인자는 냉각원 및 채널길이, 충전율, 설치 방향, 작동유체 열물성, 입력

열유속 등이 있다. 본 연구에서는 증발부가 하단, 응축부가 상단에 위치한 수직상태로 설치된 CLPHP에서 냉각 방법에 따른 성능과 유동 패턴의 비교 연구를 진행하였다. 첫 번째 실험에서는 자연 대류와 강제 대류를 냉각으로 사용할 때의 성능과 유동 변화에 대하여 관찰하고 각 냉각 조건에 따른 열유동학적 특성을 분석하였다. 두 번째 실험에서는 자연 대류를 냉각원으로 사용하는 조건에서 최적의 열적 성능을 가지는 충전율을 알아보고 유동 패턴과 CLPHP 성능과의 관계를 분석하였다.

아직까지 CLPHP의 복잡한 특성에 대하여 완전하게 이해되지는 않았지만, 본 연구를 통하여 냉각 방식 및 충전율 변화에 따른 CLPHP의 열유동학적 특성에 대한 이해가 한단계 향상되었다. 본 연구 결과는 미래의 다양한 산업 응용 분야에서 적용될 수 있는 CLPHP 설계의 기초 자료로 활용할 수 있을 것으로 기대된다.

I. Introduction

1.1. Background and previous studies

Due to the rapid development in electronics and space technologies, developing a miniature, low cost, and highly efficient heat-transfer devices are becoming more and more important. Every single conceived new design coming up in the market is with higher power dissipation levels. The dissipation is not the only problem, but the heat flux is also an important factor. The conventional heat pipes such as grooved heat pipes, sintered heat pipes, loop heat pipes, thermosyphons, and the vapor chamber played an important role in the electronics industries. Considering only the computers in the electronics industries, many manufacturers are employing heat pipe thermal solutions on their desktop, servers, laptops, and server computer opening a huge market to the heat pipe while having greater demands. The same goes for space technologies, and nuclear reactors, especially in the shuttle, where heat pipes play an important role in transferring the heat. This led to high demands on novel thermal management technologies to improve system performance, reduce complications, and improve reliability.

Akachi et al. [1] have received considerable attention for their effective solutions to these thermal problems by introducing a novel concept of heat and mass transfer device named as the pulsating heat pipe (PHP). PHPs have advantages concerning their simple structure, fast thermal response, higher heat transfer rate, and simple construction, and they have applications in heat recovery systems, electronic cooling systems, space, cryogenic, automobiles, solar and thermal energy, among others [2–5]. The PHP is divided into 3 different types: closed-loop OHP, open-loop OHP, and OHP with unidirectional valve; among them, the closed-loop OHP has a better thermal performance. PHPs have two main sections called the

evaporator and condenser sections, and their performance relies on the oscillatory/pulsatory mode of the internal working fluid between these two sections. The evaporator section is the heating section where the evaporation of liquid film or flow boiling occurs, while the condensation of the two-phase flow occurs in the condenser section. The internal complex flow patterns, ranging from the slug-plug flow to annular flow, are initiated by the interior pressure instabilities of alternative tubes, which affect the total heat flux from the evaporator to condenser sections [6,7].

Owing to its characteristics many researchers have investigated its performance experimentally and theoretically. The latest results reported by Qian [8] showed that the thermal performance of a single turn PHP increase when the heat flux is under 14,000 W/m^2, DI water has the best thermal performance (0.5 K/W): the thermal resistance is about 74% lower than that of acetone and ethanol. Considering this value, it can be understood that this heat pipe performs better particularly for the transport of heat in a long distance. The performance of the PHPs is affected by various parameters, including its structure, working fluid, operating environment, outer diameter, number of turns, total height, filling ratios, inclination angle, and condenser area [9–11]. The gravitational force also plays an important role in the use of PHPs for space applications. Ayel et al. [12] performed an experimental study on the effect of various gravity forces on closed-loop PHP (CLPHP), and they concluded that these heat pipes continue to operate even in microgravity conditions, and the thermal performance is enhanced when operated in a vertical orientation.

Comparable to a conventional heat pipe, the pressure difference between the evaporator and condenser of the PHP is imperious and must be maintained at a certain or critical value to generate a self-sustaining oscillation of liquid and vapor slugs in the heat pipe. The pipe

is filled with a working fluid to form vapor bubbles and liquid plugs (a liquid-vapor mixture) dependent on the filled ratio (Bond number as well). When the heat pipe is in process, the saturated pressure/temperature of the liquid-vapor mixture varies from the evaporator section to the condenser section depending on the operating temperature. When the evaporator section is heated, the vapor pressure increases, and liquid at this end is superheated before vaporization takes place at the wall surface. Once the vapor bubble is formed in the superheated liquid, its growth rate is very rapid, especially in a small limited space. At another cooling end of the device, when the vapor bubbles are cooled, the bubbles collapse, and the condensing bubble is formed inside the channel which moves towards the evaporator section and takes place of another bubble. The temperature of the vapor-liquid mixture is determined by the cooling surface area, wall temperature, and heat transfer coefficient in the condenser section. The pressure in the condenser is dependent on the temperature of the vapor-liquid mixture. When the liquid-vapor mixture of working fluid flows through the evaporator and condenser repeatedly, an enhanced heat/mass transfer process occurs due to the phase-change heat transfer and convection (Depends on the source). This process of the oscillating bubble-train flow is a typical non-equilibrium and transient heat transfer process.

For numerous years, studies conducted on PHPs mainly focused on the effect of various parameters, such as the dimensions, heat loads, inclination angle, operational limits, working fluids, and filling ratio (FR), on the thermal performance [13–17]. While the study of the thermal performance of PHPs was carried out broadly by numerous researchers [18–22]. Research on PHPs has recently been broadened to investigate the internal flow characteristics, such as the oscillating flow motions inside the PHPs, which affect the device performance [23–27]. The internal flow patterns of PHPs start from slug and plug flow and often reaches

the annular and semi-annular flow with higher heat loads. These internal flow patterns are the real factors that change the total heat flux and total heat transfer rate, along with the heat transfer rate from the evaporator section to the condenser section. Naturally, these flow patterns of the PHPs directly depend on the conditions and parameters of the planned experiments.

Mangini et al. [28] investigated the two-phase flow of a single loop using infrared analysis, which allows the observation of the wetting and dewetting of the liquid thin film. Several experimental and theoretical studies have been performed for microscale observation of PHPs about the thermal performance and flow regimes [29–31], broadening the research on PHPs. Although PHPs have numerous advantages over conventional heat pipes, they are not fully commercialized, as their working principle and operation conditions are not fully understood. To extend the research on PHPs, researchers conducted experiments on cryogenic PHPs, which operate at very low temperatures, i.e., 77 K, by using helium, hydrogen, neon, and nitrogen as working fluids [32–39].

In addition to these experiments, Fonseca et al. [40] designed an innovative helium-based PHP with an oscillation period of only 21 s to achieve an effective thermal conductivity. Even though most PHPs have been generally operated using condensation devices to create a restoring force, it is known that ambient conditions without any power consumption for cooling provide a sufficient condensation temperature for laboratory experiments, and several researchers have investigated the performance and working principle of PHPs at room temperature [41–44]. Patel et al. [45] investigated the influence of working fluids on the startup mechanism of a closed-loop pulsating heat pipe (CLPHP) by keeping the condenser section open to the environment to dissipate heat naturally. The onset pulsations for the

ethanol were observed at heat input power (Q in) = 40.5 W. Karthikeyan et al. [46] performed experiments on PHPs charged with deionized water by exposing the condenser section to the ambient temperature. While the initial flow oscillations were obtained at a heat load of 20 W, the working principle completely depended on the working parameters, such as the FR and the evaporator length. Similarly, Iwata et al. [47] concluded experiments on the maximum heat transfer and operating temperature of oscillating heat pipes and found that the maximum heat transfer depends on the ambient temperature.

Although the condensation strongly affects the performance of PHPs, few studies have investigated the thermo-hydrodynamic behavior of PHPs when the cooling temperature is changed or when the condenser is exposed to ambient conditions. Khandekar et al. [48] observed that the thermal resistance decreases with the increase in Qin until the cooling source reaches a state where it is unable to keep up with the heat flux. The effect of the condenser temperature (Tc) was investigated recently by Betancur et al. [49], and they have found that increasing the thermal bath temperature for the PHPs leads to early start-up pulsations. Because there is no wick structure in PHPs, it can even operate by exposing the condenser section to the ambient conditions, in which the heat is dissipated naturally. Karthikeyan et al. [46] observed the start-up pulsation at 20 W by exposing the condenser section to the ambient environment. Although various theoretical and experimental studies have been performed to obtain a fundamental understanding of the oscillating characteristics of internal flows [50, 51], there remain few studies on the development of the complete design for a particular application because of an incomplete understanding of the thermo-hydrodynamic parameters and the condensation phenomena. Detailed information on the start-up pulsations and dry-out conditions are also missing for a complete design, and hence need

to investigate for different convection sources. Therefore, it is essential to understand the flow phenomena by visualizing the internal flow patterns and investigating the bubble dynamics, including the displacement, velocities, and acceleration, with different condensing sources. The potential of PHPs can be increased by obtaining additional insight into the two-phase flow trends, which can be understood by a thorough investigation of the oscillating/pulsating motion inside the capillaries.

1.2. Pulsating Heat Pipes: Working Mechanism

PHPs are two-phase heat transfer devices that rely on the oscillatory a pulsatory motions of the working fluid. It consists of three main sections namely; Evaporator, Condenser, and Adiabatic sections as shown in Figure 1.2. The adiabatic section can be considered as optional. The device is first evacuated with vacuum pressure and then partially filled with the working fluid. Which distributes itself into liquid slugs and vapor plugs depending upon the dominancy of the surface tension over the gravitational force of the working fluids. As the PHPs are wickless and nono equilibrium heat transfer device, it works on the pulsatory motions of bubbles (vapors), when the heat is added to the evaporator section, vaporization occurs. When the heat is removed from the condenser section condensation of the vapor takes place. The volume expansion and contraction due to the liquid vaporization and vapor condensation cause the oscillatory motion of liquid slugs and vapor plugs respectively as shown in Figure 1.3. The vapor plugs move to the condenser section by a driven force from the evaporator which condensed in the condenser section and moves back by a rejection force from the condenser section to the evaporator and it takes place the position of another bubble and vice versa. [52-56].

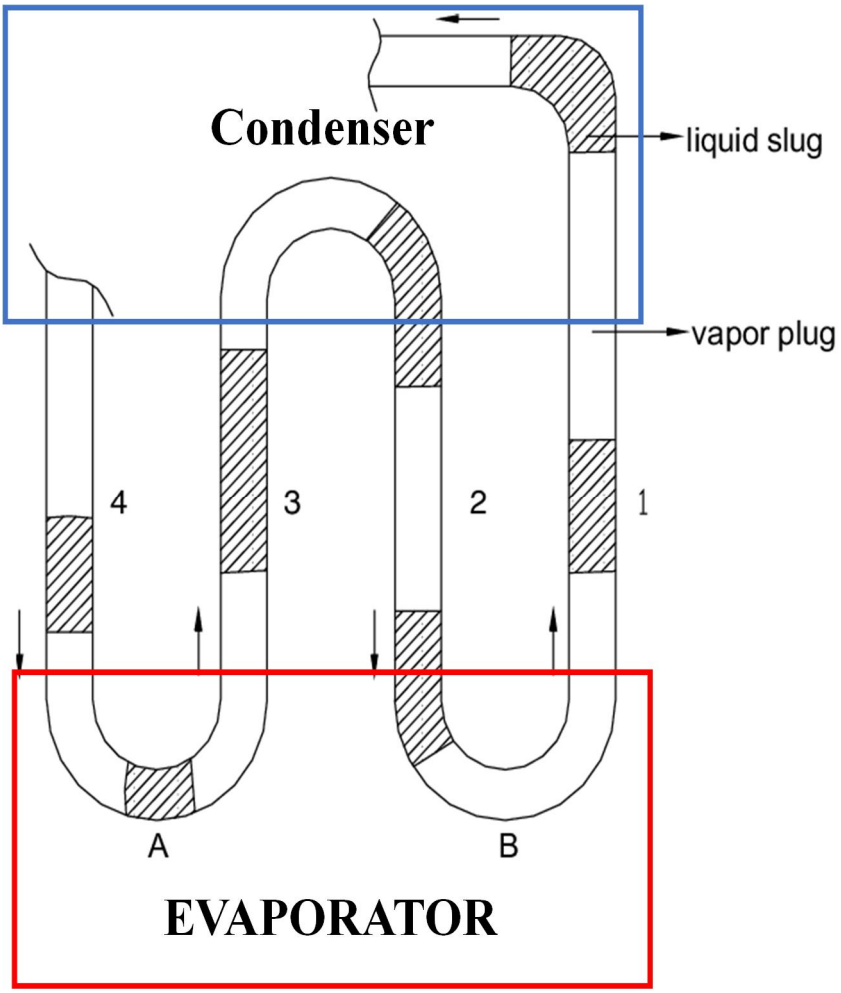

Fig 1.1. Volume expansion and contraction in evaporator and condenser zone

An actual working CLPHP is not isothermal, there is a temperature gradient between the heating and the cooling sections. Similarly, the temperature gradient also exists in the U-bend section due to local heat transfer rates. The net effect of these temperature gradients within the system causes the non-equilibrium pressure conditions which are the driven force to transport the fluid. This leads to thermally driven flow regimes (Two-phase flow) instabilities. More precisely, the evaporator pushes the vapor to the condenser section, which increases the pressure, and the condenser rejects forces these vapors to move back to the evaporator section, decreasing the pressure, In this way. A non-equilibrium state exists between the thermally vapor driven and rejection forces, that try to equalize the pressure in the system.

If the heat is continuously added to the evaporator section, the pressure fluctuations within the evaporator and condenser are disturbed and that leads the dry-out of the channels which is considered as the critical heat flux zone of the system due to the vapors cannot withstand further driving force from the evaporator section. Since the overall thermal performance is dependent upon the internal flow regimes (Two-phase flows) starting from slug/plug flows to circulatory annular flow, these flow motions are directly dependent upon various parameters such as heat load (Q), evaporator and condenser area, working fluid, internal diameter (di), device materials and cooling method. Even though several studies have demonstrated that the initial flow motions and onset pulsations depend on the device parameters and working conditions, such as the Q, evaporator length, and FR, the effects of these factors on the flows and corresponding thermal performance are not yet fully understood because the flow is complex in PHPs and is influenced by various parameters. Therefore, more fundamental studies on the flow characteristics are required.

An attempt has been made to recognize, evaluate, and asses the relative importance of the major influence of these parameters, by visualizing the thermally driven flow regimes of the CLPHP and characterizing its thermal performance.

1.3. The motivation for the present research

In the wake of current tendencies, the demands from the present-day thermal solutions of electronic equipment are, its lower thermal resistance, higher heat transfer efficiency, heat transport capability, long term reliability, and low cost. This required a proper cooling system to achieve a stable functional device. Whereas the primary goal of any cooling system is to enhance the set or module performance and consistency, which are the stronger functions of temperature depending upon the cooling source. The temperature has a great

role in the device functionality (because many materials are temperature-dependent), device safety (should be considered as the browse through rule for laboratory, components and human risks factor), and device failure (physical failure). Various modern electronics cooling are introduced which are primarily divided into the two:

- **Active cooling**: by using the external energy to cool something (device) such as fans, cooling chambers, etc. refers to the natural convection. (Proper care should be taken in the selection of working fluid).
- **Passive cooling**: opposed to active cooling which uses no energy to cool the system in that case an ambient surrounding is enough to circulate coolant to transfer the heat from one place to another place. Refers to forced convection.

These technologies are widely used for convection with a single phase. In addition to that, a phase change heat transfer is used for two-phase, which primarily includes the flow boiling, and pool boiling technologies as shown in Figure 1.2. One can see that the heat transfer coefficient is much higher using the phase change heat transfer technique.

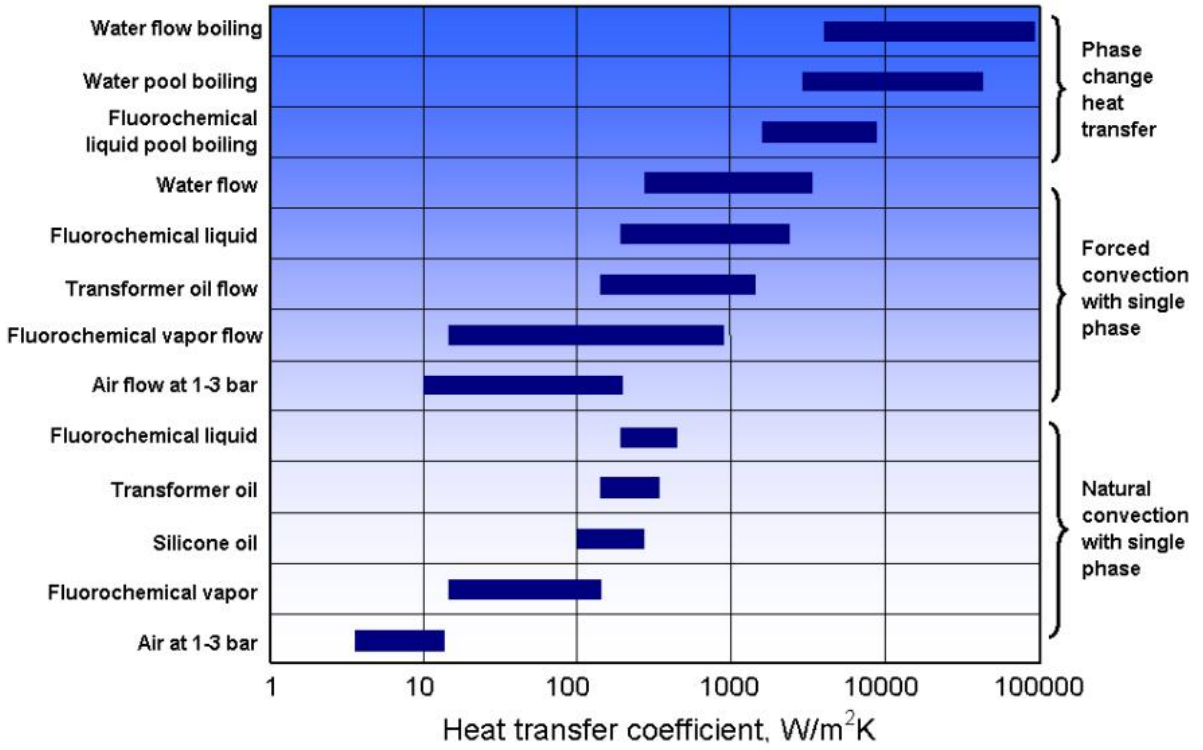

Fig 1.2 Heat transfer coefficient with phase change

In addition to that, the physical properties of the working fluid also play an important role, to cool the system. With the boundary conditions in mind, novel cooling approaches are continuously being established. Similarly, materials development and its characterization also improved the performance of the system. Constant rigorous demands led to the development of phase change techniques such as pool boiling, flow boiling, impingement jet cooling, and microchannels flow boiling concepts. In parallel, the heat pipes in various fields and designs have played an important role in many cooling applications. The introduction of heat pipes (micro) has led to the development of many hybrid-cooling concepts combining different levels of cooling [57].

Pulsating heat pipes (PHPs) is another novel concept proposed by akachi [1] as shown in Figure 1.3, which meets al the present-day cooling requirements. PHPs already found applications in the micro, power electronics, and space applications owing to its unique

characteristics and low costs. However, its complexity in the thermo-hydro dynamics coupling is unique and therefore required and completely different research outlook to understand its performance with different cooling techniques and working fluids along with filling ratios (FR). Besides, the overall performance is dependent upon the internal flow behaviors of the working fluid inside the device. It is possible to understand that the device is performing well with certain working fluids and cooling techniques but the question is why?. To recognize that, one must comprehend the flow dynamics of the working fluid inside the heat pipe. For that purpose, the flow visualization technique is highly appreciated.

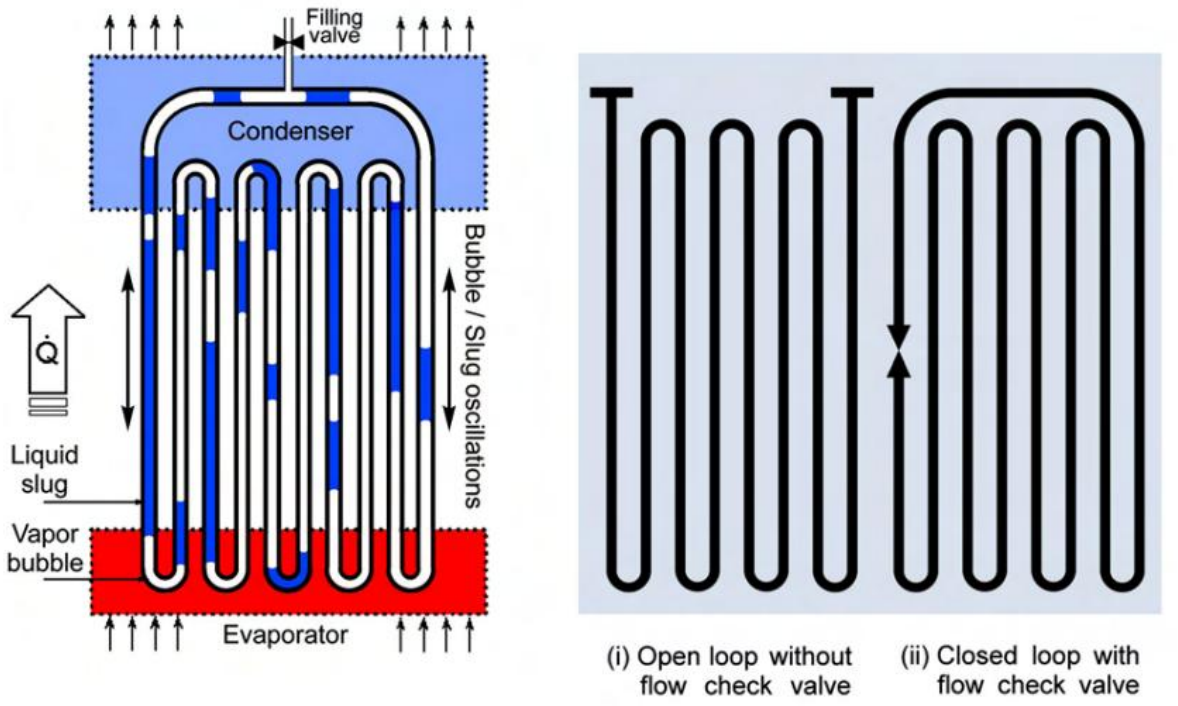

Fig 1.3. Pulsating heat pipe

The present research aims to understand the fundamental thermo-hydrodynamics operational characteristics of Closed-loop pulsating heat pipes (CLPHPs), details of which will be presented in the subsequent chapters. The thermal performance is studied for different working fluids and cooling techniques with the aid of a series of visualization experiments (to understand

the thermo-hydrodynamics behaviors), heat transfer measurements, bubble displacement, velocities, and accelerations. The attention is focused on the inter-relations of bubble behaviors and heat transfer characteristics when the device is exposed to ambient/natural cooling and active cooling. Experiments are performed on different working fluids and operating parameters which will be presented in the experimental setup/ methodology and results in sections. Although such a comprehensive design is still not complete, it is strongly believed that this work will provide a benchmark for understanding the bubble behaviors and its inter-relation with heat transfer characteristics and cooling strategies for different industrial applications and will provide and concrete foundation for the future research direction.

Before proceeding further, an explanatory working mechanism of PHPs is presented so that the concept can be better appreciated in the context of cooling technologies.

II. Description of experiments

The following system briefly describes the common peripheral devices used in all of our experiments. It includes the data logging system, high-speed camera, power supply, and convection sources. Thereafter, a brief description of the setup and methodology follows.

2.1. Common peripheral devices

All of the experiments are performed with the following common peripheral devices.

2.1.1. Data acquisition system

In each experiment, cDAQ-9171 bus-powered compact data acquisition system was employed;

(4)32-bit general-purpose counters, with analog input FIFO size of 127 samples. The DAQ was a USB chassis that is designed for the small, portable sensors measurements. Combined with cDAQ-9171 the NI 9211 (4TC, 80mV, 24 Bit, 14 S/s aggregate) sensor (thermocouple) input module was used for high accuracy thermocouple measurements. The sensor programming was done by using Ni LabVIEW SP1 software using a personal computer. A special program was developed in the NI LabVIEW software to retrieve the raw temperature readings with auto-save mode after 20 minutes. In our case since we are detecting the temperature data, all the temperature data was measured with K-type thermocouples with the accuracy of ± 1 ° C, which were employed on either side of the evaporator and condenser section. Figure 2.1 represents a common DAQ system used in each experiment.

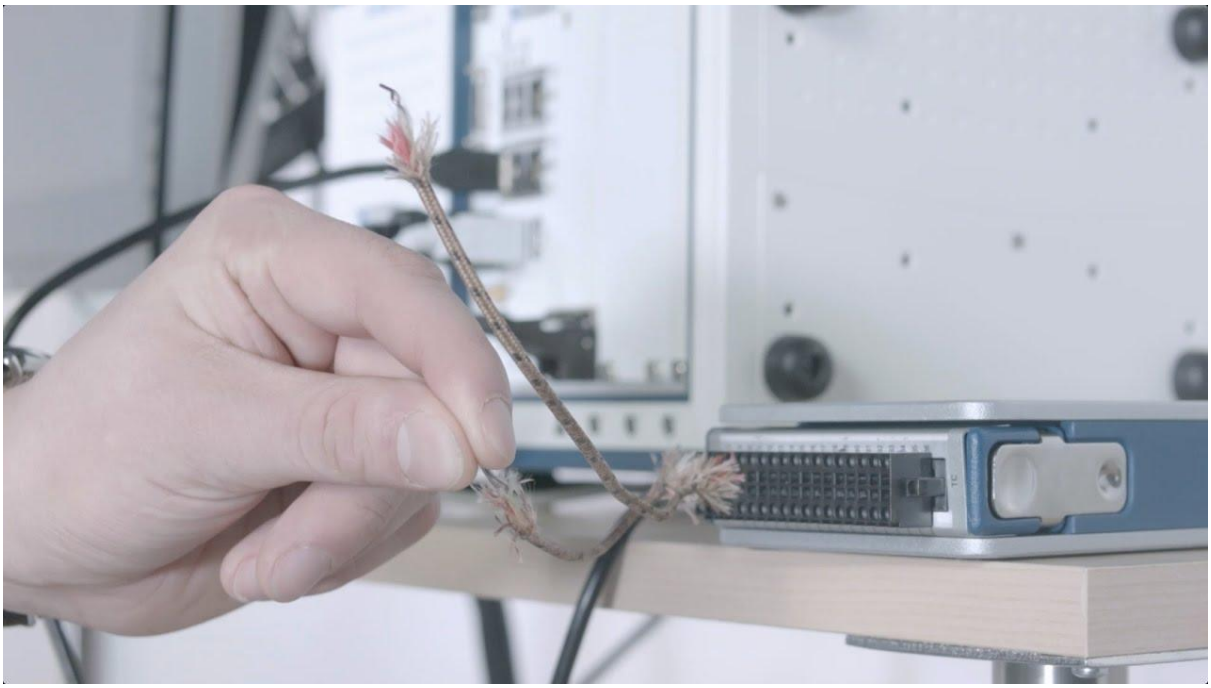

Fig 2.1. DAQ system with thermocouples

2.1.2. High-speed camera

For obtaining complete motion pictures and videos of the flow behaviors and its pattern

identification a high-speed (Fastcam Mini UX50, Photron, USA) camera was used. This camera had a sensor with a maximum resolution of 1280 ×1024 112 pixels at 2000 frames per second (fps), which has the Pixel size of 10 μm×10 μm) with the optical lens and was placed in front of the CLPHP. The flow patterns are then identified using a Photron FASTCAM 115 viewer software. In order to obtain the bubble displacements and velocities, a correlation tracking algorithm is employed in a Photron FASTCAM Analysis software. To better understand the CLPHP, all of the collected data are post-processed to enhance the visualized images using adobe photoshop and Image J. The picture of the high-speed camera and the images obtained from this camera are presented in later sections.

2.1.3. Convection Sources

In order to cool the device, two types of convection sources are used for two different experiments. In one experiment, the performance of CLPHP has been analyzed by natural convection i.e. the condenser area was exposed to air-conditioned room temperature (25 ±5 ° C) and hence the convection occurs naturally. While in another experiment for the comparative analysis on CLPHP for natural and forced convection, air-conditioned room temperature (25 ±5 ° C) and a DC-Fan was used respectively. The pictures of which are being presented in other chapters.

2.1.4. Power supply

In each experiment, a power supply is used to give the stepwise heat to the evaporator section of CLPHP, which was connected to the nichrome wire (Heater). In one experiment a PL-300D-Protek, 60V 10A was used and in another experiment, a direct current (DC) power supply (Toyotech TDP-3020B, 30V-20A) was used. Proper care was taken while

using the power supply fo human factor and laboratory risks. The desired amount of current (A) and voltage (V) was used in each experiment by step-wise.

2.2. Experimental setup and methodology

In this study, two experiments and their setup are explained precisely for each experiment. Based on the application background of CLPHP, all of the experiments were carried out in vertical bottom heating mode, where the CLPHP performs better under normal gravity conditions [25]. This should be considered as the starting point of the research, as the literature revealed that there is much ambiguity concerning the operation of the CLPHP. For visualizing the flow patterns, the need for the setup of visualization was strongly felt to understand the thermofluidic trends in the CLPHP. The current study can be valuable for evaluating the bubble dynamics and its trends with increasing heat loads. For that purpose, a two-turns CLPHP was fabricated and designed from a borosilicate glass tube. A whole device was fabricated as a transparent tube and then the bubble trends can be approximated when different materials are used for the device. Since there are two experiments in this study the common details for both experiment are explained as follows,

Experiment 1:

The internal diameter (di) of the glass tube was 2mm which was selected by the bond number equation and the outer diameter (do) was selected as 6mm as follow,

$$D_{Crit} \approx 2.\sqrt{\frac{\sigma}{g.(\rho_{liq} - \rho_{vap})}} \quad (1)$$

An experimental setup was designed to recognize the thermo-hydrodynamic coupling inside a

CLPHP in a laboratory, as shown in Fig. 2.2(a). The experimental set-up consists of a two-turn borosilicate glass tube CLPHP, whose schematics are shown in Fig. 2.2 (b). The laboratory experimental set-up and the condenser is shown in Fig. 2.2(c). The detailed geometric parameters and working conditions are represented in Table 2.1.

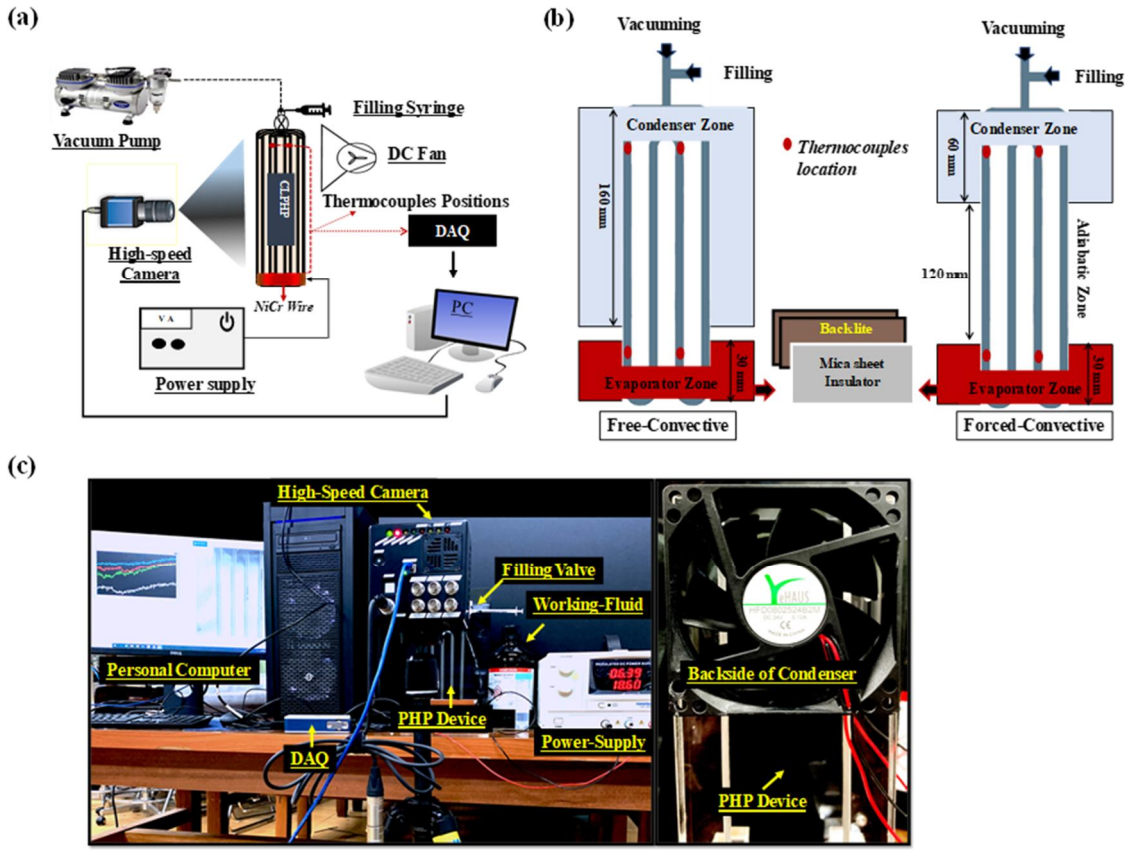

Fig 2.2. (a) Experimental layout, (b) schematics of the devices for free and forced convective operations and (c) picture of the laboratory experimental set-up.

Table 2.1. Experimental conditions and parameters.

Parameters	Free-CLPHP	Forced CLPHP
Total height	210 mm	

Total width	60 mm	
Evaporator section	30 mm	
Condenser section	160 mm	60 mm
Total volume	2.3 mL	
Inner diameter	2 mm	
Outer diameter	6 mm	
Working fluid	Methanol	
Working environment	Natural Convection	Forced Convection

A DC fan was used for cooling in the forced convective CLPHP operation. The condensation length in the forced convective CLPHP operation was 60 mm. The evaporator length was considered to be the same for both free and forced operations and was 30 mm. A black lite and mica sheet insulator was used in the evaporator region to minimize the heat loss from the system to the surroundings. Four K-type thermocouples (Accuracy ±1 ° C ±0.5%) were used, with two being placed in each evaporator and condenser section. The effect of active and passive cooling phenomena is shown in Fig 2.3. It can be noticed that a DC fan is used as forced convection for active cooling while the ambient conditions are employed as free convection for passive cooling. A 50% FR methanol was used as a working fluid. A nichrome chromium wire was mounted in the evaporator section which was made as 30 mm.

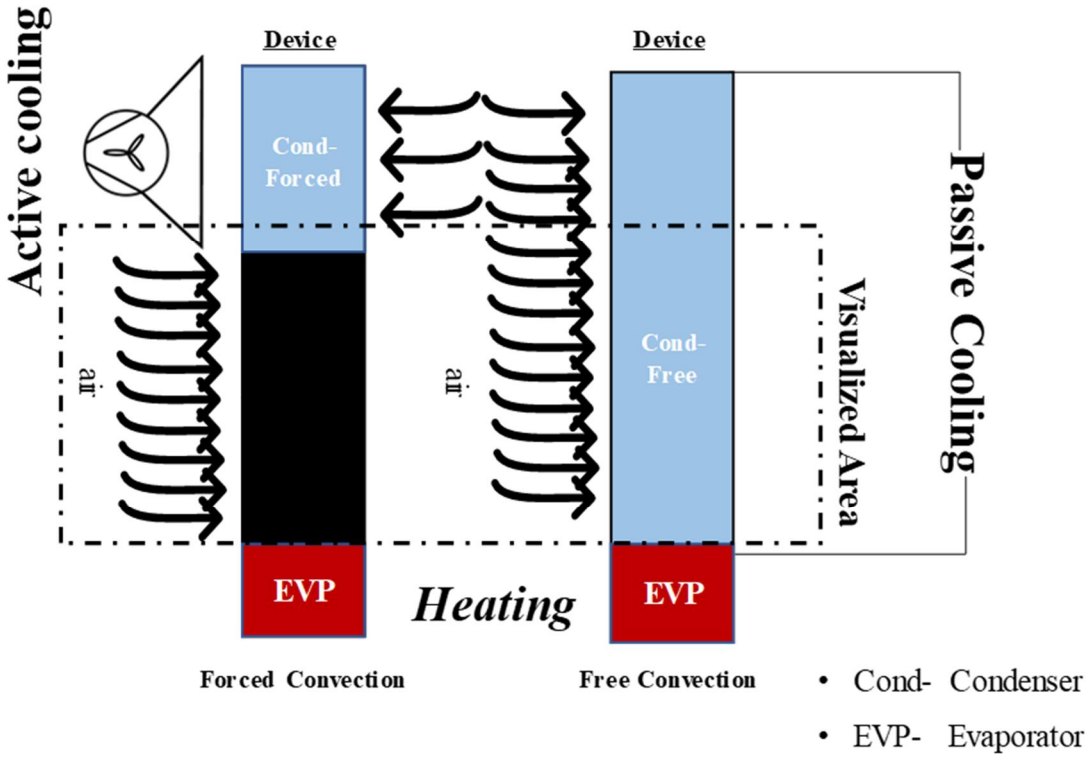

Fig 2.3. Schematic for free and forced convection as an active and passive cooling

Experiment 2:

The diameter of the PHPs significantly affects the overall performance of the system. In particular, the internal diameter of the pipe directly affects performance. Similar to experiment 1, the di and do were 2mm and 6mm respectively selected by equation one. Ethanol was used working fluid in this experiment, Figure 2.4 shows the experimental setup consisting of a two-turn glass-tube CLPHP (GT-CLPHP) device with the possible module for the evaporator and condenser sections. The glass tube (borosilicate glass) was selected to fully visualize and understand the flow phenomena in the PHP, particularly the flow from the evaporator section. The schematic of the GT-CLPHP, thermocouples location, and its dimensions are shown in Figure 7(a). Also, the layout of the overall experimental setup is provided in Figure 2.3(b). The overall length of the device is 210 mm. The evaporator section measures 50 mm, and

the remaining of the device is exposed to the air-conditioned room temperature 25℃ ± 5 ℃ and viewed as the condenser section measuring 160 mm.

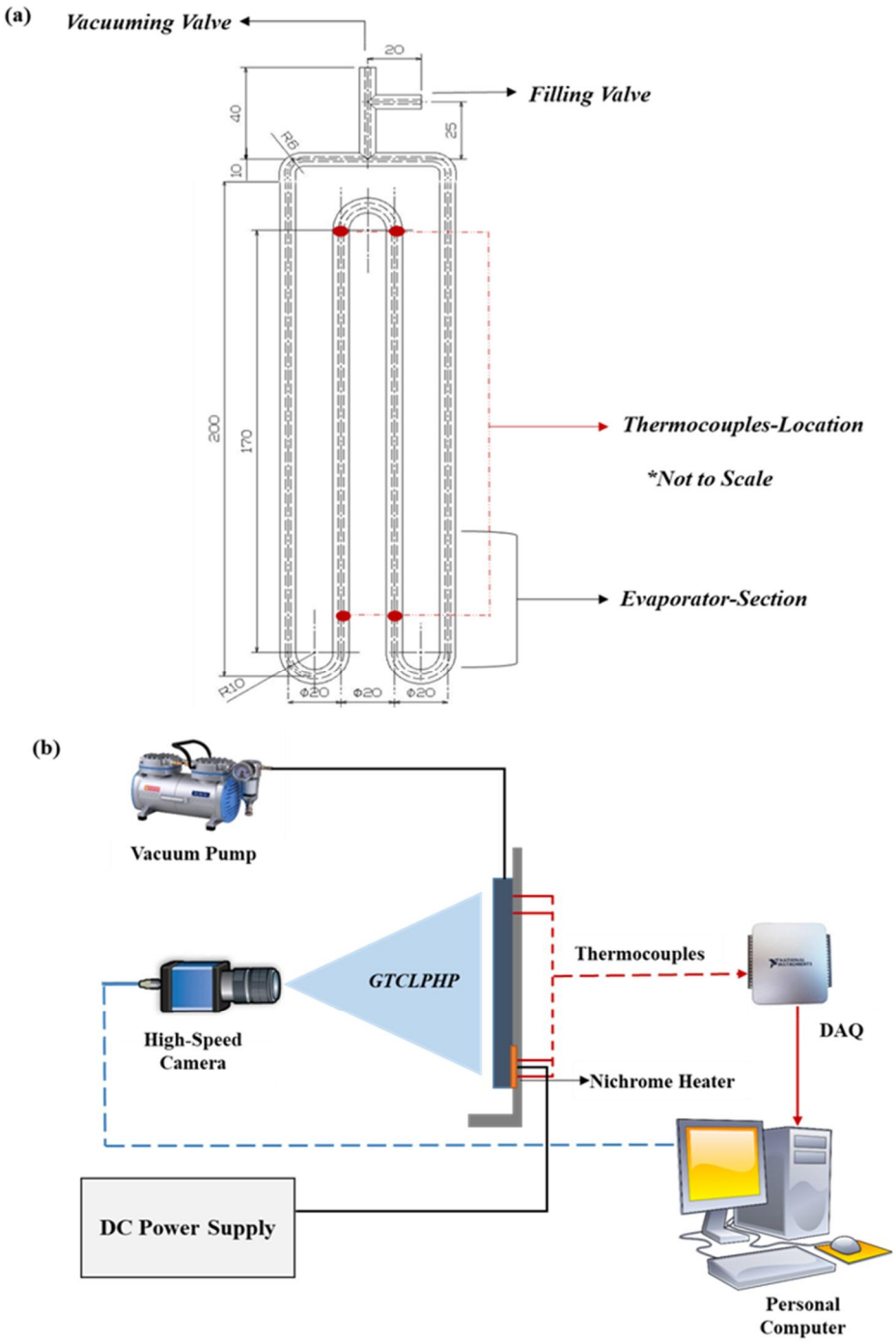

Fig 2.4. (a) Schematic of the glass tube and thermocouple positions (b) Experimental layout

In the evaporator section, a nichrome electrical wire is wound on the outer surface of the

GT-CLPHP as a heater with a distance between each wound of 5 mm. The overall setup is mounted in a vertical gravity direction. The input power to the evaporator section is provided by the DC power source (Toyotech TDP-3020B, 30V-20A). A three-way stop cock valve is used for vacuuming and for filling the GT-CLPHP.

A 10 mL non-pyrogenic syringe (BD precisionGlide™needle) attached to a three-way is used to fill the GT-CLPHP based on the required FR. Similarly, a rotary vacuum pump (rocker-300, AC110 V, 60 Hz) is attached to the vacuuming valve for the evacuation of the system. Four K-type thermocouples (accuracy ±1 ° C ±0.5%), two on either side of the evaporator and condenser sections are attached in order to measure the temperatures. These thermocouples are connected to the data acquisition system (DAQ, NI-cDaQ- 9171), which store temperatures data. The DAQ system is controlled using Ni LabVIEW SP1 and a personal computer.

The geometrical parameters and main features of the overall device are summarized in Table 2.2

Table 2.2 Geometrical parameters and main features for experimental conditions

Total height	210 mm
Total width	60 mm
Evaporator section	50 mm
Condenser section	160 mm
Total volume	2.3 mL
Inner diameter	2 mm
Outer diameter	6 mm
Working fluid	Ethanol

Working environment	Room and ambient

For both of the experiments the following steps are followed,

- Before setting the power supply to begin generating heat, the CLPHP was first evacuated by the vacuum pump under the vacuuming pressure of ≤ 5 kPa for 15 min, to remove non-condensable gases.
- The vacuum valve is then closed, and working fluid is charged into the CLPHP through a gas-tight syringe with proper care.
- After reaching the desired filling ratio, all of the valves are closed, and the system is then allowed to achieve its steady state for 30 min.
- The thermal performance of the CLPHP is calculated using the evaporator temperature (T_e) and T_c of the system.
- The data acquisition system (DAQ-NI-cDAQ-9171) is used to obtain the data from thermocouples, and log it on the PC.
- Afterward, the Q_{in} to the system is provided step-wise by setting the power supply which is attached to the evaporator section
- The high-speed camera was turned on to capture the internal flow regimes for each Q.
- During first experiment for forced convection, before applying heat to the evaporator section, a DC fan was kept on, while during the free convective operations, the condenser area is exposed to the ambient environment where the condensation occurs naturally.
- The power supply was turned off when the system accomplishes the dry-out.

2.3. Numerical data extraction and uncertainty analysis

All experiments need equation from to extract the data for the desired calculations, while all scientific experiments are subjected to a variety of errors, which leads to a difference between the actual and the measured values, in the current study for both of the experiments the following equations are used to extract the numerical data and uncertainty analysis,

The thermal performance of the system is calculated by evaluating the average $\overline{T}_e$ and $\overline{T}_c$, as expressed in Eqs. (2) and (3).

$$\bar{T}_e = \frac{1}{2}\sum_{i=1}^{2} Ti \quad (2)$$

$$\bar{T}_c = \frac{1}{2}\sum_{i=1}^{2} Ti \quad (3)$$

The total heat load is calculated using Eq. (4).

$$Q_{tot} = V \times I \quad (4)$$

where V is the applied voltage and I is the corresponding current, therefore, the total heat input is the product of V and I.

The heat loss (Q_l) to the surrounding environment was estimated from the difference between the evaporator and atmospheric temperature, which was observed at each steady-state. Because the evaporator section is properly insulated, this temperature difference was found in a smaller amount. The heat gain (Q_g) in the evaporator and the heat loss (Q_l) are calculated by the rate of temperature increase when the device is started. The Q_g and Q_l are calculated using Eq. (5) and (6).

$$Q_g = C_p \frac{\Delta T_{evap}}{\Delta t} . m_{evaP} \quad (5)$$

where C_p is the specific heat of borosilicate glass, m_{evap} is the mass of evaporator and ΔT_{evap} is temperature difference during time Δt before reaching steady-state. Then, the Q_l is obtained as follows:

$$Q_l = Q_{tot} - Q_g \quad (6)$$

The heat loss ratio (μ) was calculated by the following equation:

$$\mu = \frac{Q_l}{Q_{in}} \quad (7)$$

To estimate the actual heat input, the Q_{loss} is subtracted from Q_{tot}, as expressed in Eq. (8). Then, the thermal resistance (R_{th}) was measured based on Eq. (9).

$$Q_{in} = Q_{tot} - Q_{loss} \quad (8)$$

$$R_{th} = \frac{\bar{T}_e - \bar{T}_c}{Q_{in}} \quad (9)$$

The standard uncertainty in the Q_{in} for free and forced convection is calculated from Eq. (10).

$$\frac{\Delta Q_{in}}{Q} = \sqrt{\left(\frac{\delta V'}{V}\right)^2 + \left(\frac{\delta I'}{I}\right)^2} \quad (10)$$

Here, the maximum V by the power supply is 30V and I is 5amp. The accuracy of the ammeter and voltmeter is 0.5%. The total uncertainty for Q_{tot} in free and forced convection are ± 1.88% and ± 1.0% W, respectively. Then, the uncertainty in R_{th} is calculated from Eq. (11).

$$\frac{\Delta R_{th}}{R_{th}} = \sqrt{\left[\left(\frac{\Delta T_e}{T_e - T_c}\right)^2 + \left(\frac{\Delta T_c}{T_e - T_c}\right)^2 + \left(\frac{\Delta Q_{in}}{Q}\right)^2\right]} \quad (11)$$

where ΔT_e and ΔT_c refer to the accuracy of thermocouples, which is taken as 1 ℃. T_e and T_c represent the minimum temperature difference between evaporator and condenser during the test, and this temperature difference is 28.5 ℃ and 37.5 ℃ for free and forced convections respectively.

The results obtained from these equations are based on real-time experiments while two different tables are made to categorize the error and Q_l from both experiments. Table 2.3 and 2.4 represents the Q_l and uncertainty analysis for experiment 1 respectively, while Table 2.5 and 2.6 represents the Q_l and uncertainty analysis of experiment 2 respectively.

Table 2.3. Minimum and maximum heat loss and heat gain by the PHP when total heat is given during experiment 1.

Source	Total Heat (Q_{tot})	Heat Gain (Q_g)	Heat Loss (Q_l)	Heat Loss Ratio (%)
Free Convection	6-50	5.91-49.17	0.09-0.83	1.5-1.66
Forced Convection	6-80	5.88-78.79	0.12-1.21	2.0-1.51

Table 2.4. The minimum uncertainties in the results for both free and forced convection during experiment 1.

Quantity	Uncertainty	
	Free Convection	Forced Convection
Temperature	0.25% ℃	0.25% ℃

Voltage	±0.62% V	±0.53% V
Current	±1.2 A	±0.87 A
Pressure	±0.1 kPa	±0.1 kPa
Filling Volume	± 0.1 mL	± 0.1 mL
Heat Input	± 1.88% W	± 1.0% W
Thermal Resistance	± 1.82% ℃/W	± 1.07% ℃/W

Table 2.5. Heat loss and heat gain by the PHP for experiment 2.

Filling Ratio FR (%)	Heat Load Q_h (W)	Heat Gain Q_C (J/s)	Heat Loss Q_l (J/s)	Heat Loss Ratio μ (%)
20	10-50	9.93-49.93	0.06-0.07	0.6-0.14
30	10-50	9.89-49.94	0.10 -0.06	1.0-0.11
40	10-50	9.82-49.98	0.17-0.02	1.7-0.04
50	10-50	9.94-49.95	0.05-0.05	0.5-1.00
60	10-50	9.95-49.96	0.04-0.03	0.42-0.06

Table 2.6. Maximum uncertainty in the measurement system for thermal resistance for experiment 2.

Quantity	Uncertainty
Temperature	±0.25%
Pressure	±0.1 kPa
Voltage	±0.1 V
Current	±0.01 A
Filling volume	±0.1 mL
Thermal resistance	±7.5%

In experiment 1, the heat transfer characteristics are measured to compare the performance

for free and forced convection and hence the effective thermal conductivity (K_{eff}) and the effective heat transfer of the evaporator (h_{eff}) were calculated using Eqs. (12) and (13) for both free and forced convective CLPHP operations, respectively.

$$k_{eff} = \frac{L_{tot}}{A_{cr}}\left[\frac{Q}{\Delta T}\right] \tag{12}$$

where L_{tot} is the distance from the evaporator to the condenser section, and A_{cr} is the total CLPHP cross-section area.

$$h_{eff} = \left[\frac{Q_{in}}{A_{ax}(\Delta T)}\right] \tag{13}$$

where A_{ax} is the overall evaporator cross-section area calculated by Eq. (14).

To measure the radial and axial heat flux, a single U-turn section in the evaporator section is selected, as shown in Figure. 2.5. Then, the axial and radial heat fluxes are calculated by considering the axial (A_{ax}) and radial (A_{rad}) areas as in Eqs. 14 and 15.

$$A_{ax} = N\frac{\pi.\mathrm{di}^2}{4} \tag{14}$$

$$A_{rad} = N.\pi.d_i\left[l_{e*} + \frac{1}{2}\pi.R_m\right] \tag{15}$$

where N is the number of turns and d_i is the inner diameter. l_e and R_m are the length of the straight part and the mean radius of the curved part, respectively. Then, the amount of heat flux is calculated by Eq. 16.

$$q'' = \frac{Q_{in}}{A} \tag{16}$$

where Q is the heat applied to the evaporator, and A is the corresponding radial and axial

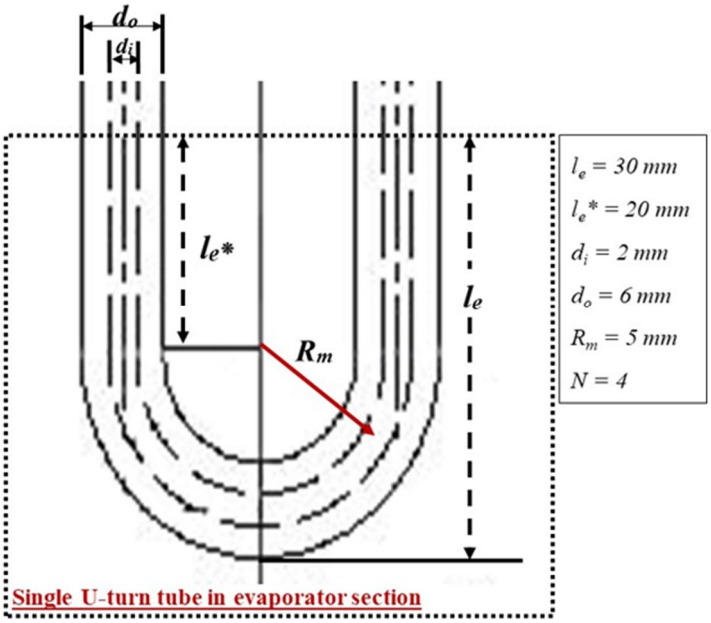

Fig. 2.5. Evaporator area for the calculation of radial and axial heat fluxes.

areas.

3. Results and Discussions

3.1. Experiment 1 (Effect of active and passive cooling on the thermo-hydrodynamic behavior of CLPHP)

In this experiment, the effect of active and passive cooling on the thermo-hydrodynamics of CLPHP has been investigated, the active cooling was done using forced convection while the passive cooling was done by free convection. The results take into account the effect of convection sources on the start-up pulsations, dry-out conditions, critical heat flux, thermal performances, flow regimes, and bubble behaviors of CLPHP using a uniform heating pattern.

The following results are obtained from the experiments, based on the result the study can be helpful to design and develop a CLPHP based on its thermo-fluidics properties for engineering applications.

3.1.1. Effective operating ranges of CLPHP

Figure 3.1 represents the variations of T_e and T_c. The uniform heat flux was provided step-wise by regulating the power supply, which was turned off when the system reached the dry-out state. The external source for the condenser section significantly affects the operating temperature of CLPHP. The temperature trends for both T_e and T_c were common in the perception of increasing with the increase in Q_{in}. Figure 9(a) represents the T_e and T_c for the natural convection operating condition. The initial start-up pulsation is observed at Q_{in} values of 24 W (q''_{ax} = 191 W/cm^2, q''_{rad} =3.42 W/cm^2). The value of T_e is drastically increased with the increase in Q_{in}. The dry-out is observed from the dry-patch in the evaporator section, and it can be predicted from the sharp rise in T_e because the heat cannot be removed from the evaporator section, which increases the surface temperature. The dry-out for the free convective CLPHP occurs at a Q_{in} value of 50 W (q''_{ax} = 398 W/cm^2, q''_{rad} =7.14 W/cm^2). Because there is no external source for the condensation, T_c depends entirely on the natural convection and internal two-phase flow [23]. The operating range is narrow for the free convective CLPHP owing to the delayed start-up (24 W) and quick dry-out (50 W) conditions compared to the forced convective CLPHP shown in Fig. 3.1(b). The initial flow motion for forced convective CLPHP was observed at a Q_{in} value of 12 W (q''_{ax} = 95 W/cm^2, q''_{rad} =1.71 W/cm^2) when a little flow motion (bubble nucleation) occurs in the evaporator section. However, for forced convective CLPHP, the start-up of pulsations was observed at Q_{in} of 18 W (q''_{ax} = 143 W/cm^2 q''_{rad} = 2.57 W/cm^2). The initial dry-out occurs late at Q_{in}

value of 80 W (q''_{ax} = 636.94 W/cm^2 q''_{rad} = 11.43 W/cm^2). The corresponding start-up pulsations and dry-out condition are indicated in Fig. 3.1(b) for forced convective CLPHP operations. The operating range is broader in forced convection owing to the initial start-up and delayed dry-out. At lower values of Q_{in}, there is no specific change or slow increase in T_c during forced convection. Because the number of U-turns is two, the possibility of stop-over phenomena increases, especially for lower Q_{in} [26].

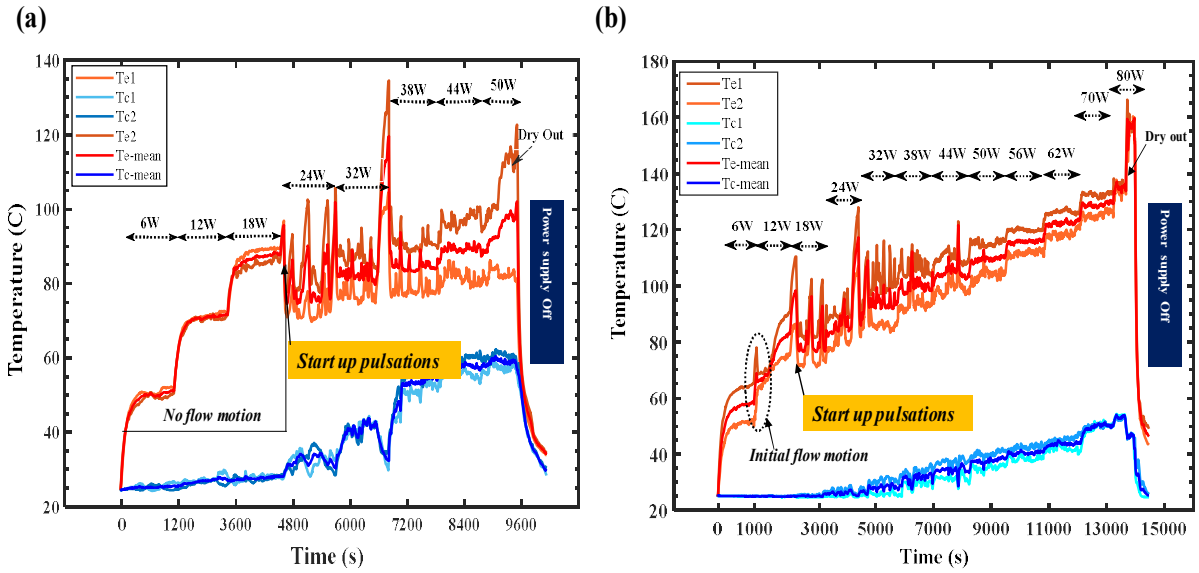

Fig. 3.1. Evaporator and condenser temperature responses at (a) free and (b) forced convective CLPHP operations.

3.1.2. Temperature response for various operating modes

The effects of Q_{in} and the internal flow patterns on T_e and ΔT_e are analyzed for the start-up pulsations, regular pulsations/oscillations, and dry-out conditions for both free and forced convection. Figure 3.2 shows the effect of internal flows on T_e during different operating modes for free convection. During start-up pulsations, the stop-over phenomena were dominant owing to the imbalanced force and fewer turns. Therefore, in Fig. 3.2(a), the initial

temperature difference is higher (12.11 ℃) when the flow stops, as indicated by a red dot. The temperature difference decreases to 2.9 ℃ when the oscillations become regular. For regular oscillations, the temperature difference lies within the range of 0.05–1.02 ℃, as shown in Fig. 3.2(b). These temperatures indicate the bubble motion inside the tubes for one time period of evaporation and condensation, i.e., when the bubbles are driven from the evaporator section, a new bubble takes its place owing to the restoring force from the condenser and vice versa. This means that a lower temperature difference is due to the faster oscillations, and a higher temperature difference is caused by slow oscillations during the regular pulsation mode. The temperature difference increases sharply during dry-out conditions because there is an insufficient amount of fluid that can transfer heat leading to the normal operation condition. A similar study was performed for the forced convective CLPHP. Figure 3.3 represents the effect of Q_{in} on the temperature of the different operating regimes for forced convection. When the initial pulsations are observed, the temperature decreases drastically by 21.05 ℃, as shown in Fig. 3.3(a). During regular pulsations, the bubble motion inside the capillaries is faster, which leads to a temperature difference of ± 2 ℃, while when dry out occurs, the temperature increases sharply, as shown in Fig. 11(c).

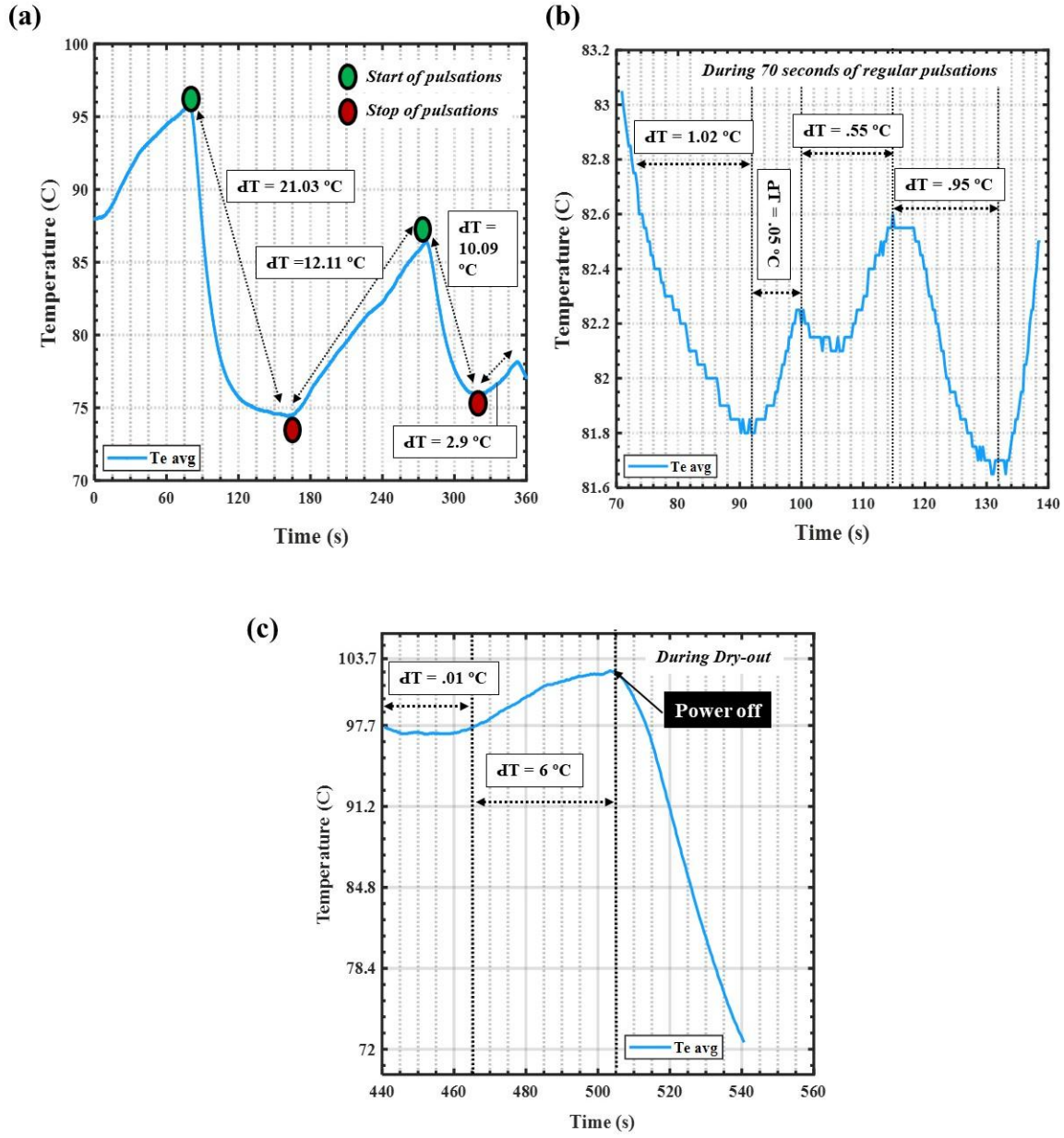

Fig 3.2. Variations of operating temperatures for free convective CLPHP during (a) Start-pulsations, (b) normal operating regimes, and (c) dry-out.

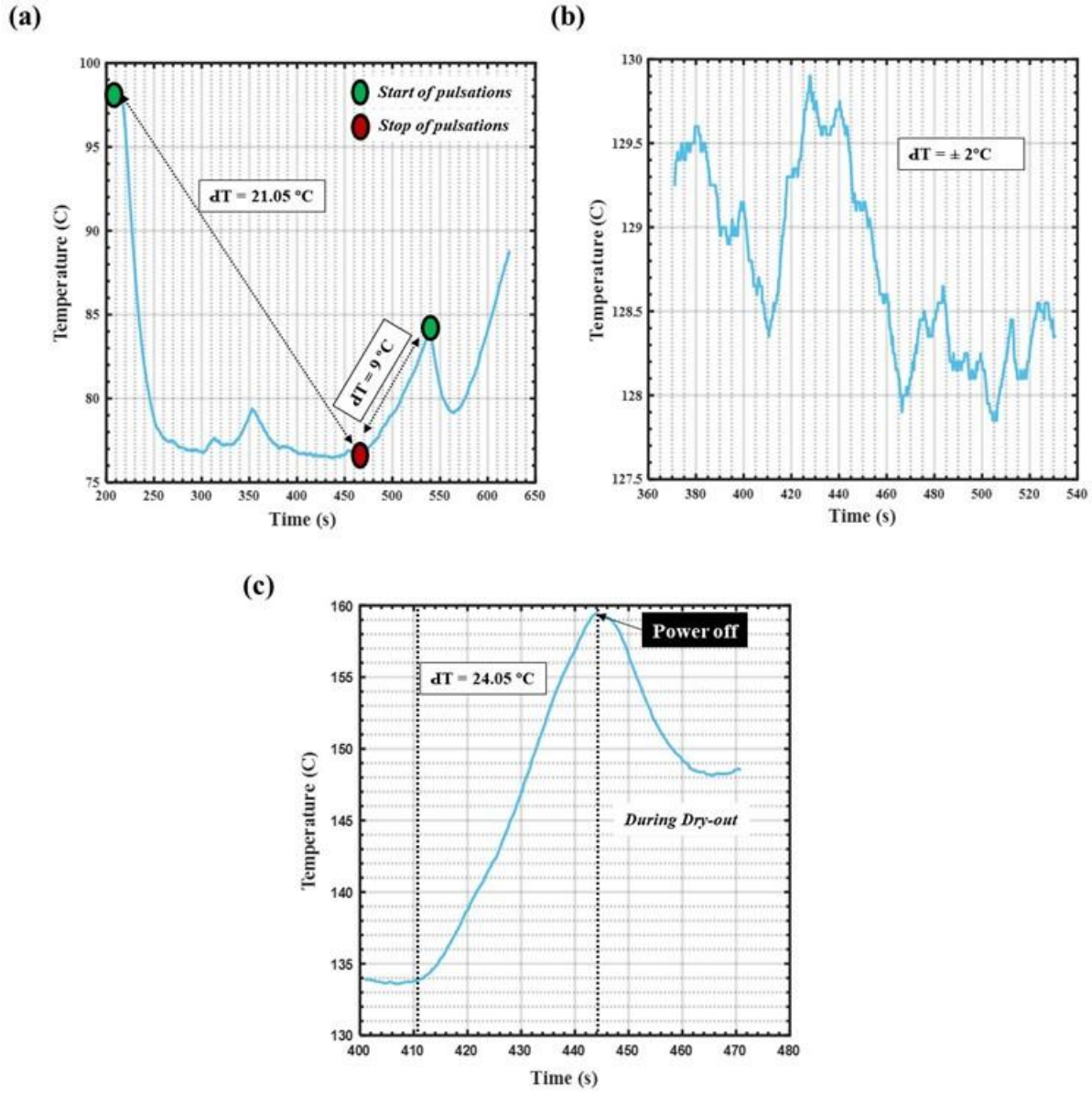

Fig 3.3. Variations of operating temperatures for forced convective CLPHP during (a) Start-up pulsations, (b) normal operations, and (c) dry-out.

3.1.3. Thermal performance comparison

The performance of the heat transfer process is generally identified by an evaluation of R_{th}. The stronger the heat transfer process, the smaller the value of R_{th}. For the smaller R_{th}, the T_e and T_c values must be closed to each other; thus, a more efficient CLPHP can be obtained. The R_{th} is also dependent on the value of Q_{in} of CLPHP. Because the heat transfer

in CLPHP is caused by the fluid flow between the evaporator and condenser section, the flow inside capillaries and R_{th} are inter-related. Figure 3.4 shows a typical R_{th} curve, where the blue and the red curves represent the R_{th} through forced and free convective CLPHP, respectively. The value of R_{th} for both free and forced convections decreases with the increase in Q_{in}. The operating range is short for free convection, but the performance is higher. The device performs better with a heat flux rate of q''_{ax} = 191 W/cm^2, q''_{rad} =3.42 W/cm^2 to q''_{ax} = 350.31 W/cm^2, q''_{rad} =6.28/cm^2 when the condensation occurs by natural convection. For a Q_{in} value of 24 W (q''_{ax} = 191 W/cm^2, q''_{rad} =3.42 W/cm^2), the onset of pulsations occurs, which decreases R_{th} very rapidly; this indicates the enhancement of the heat transfer through the fluid motion. The rate of internal fluid phase is greater in free convection because there is no external source for condensation. Therefore, T_c increases dramatically with an increase in Q_{in}, which has a very small difference in T_e and T_c. Because of this small difference, R_{th} decreases from 3.72 ℃/ W to 0.42 ℃/ W for Q_{in} values ranging from 6 W to 50 W. As shown in Fig. 12, the value of R_{th} for forced convection also decreases with an increase in Q_{in}. However, the lowest R_{th} was 0.85 ℃/ W, which was achieved at Q_{in} of 80 W (q''_{ax} = 636.94 W/cm^2, q''_{rad} =11.43/cm^2). In the case of forced convection, the difference between T_e and T_c is a little greater than that in free convection because the condensation takes place actively owing to the external DC fan. However, the operating range increases owing to the higher heat rejection rate for active condensation. By evaluating R_{th} with free and forced convection, it can be understood that the free convective CLPHP is efficient for lower Q_{in}, while the forced convective CLPHP is more efficient for higher Q_{in}. It should also be noted that the performance can be enhanced when more than two U-turn CLPHP is used because the majority of heat is transferred by specific and latent

heat.

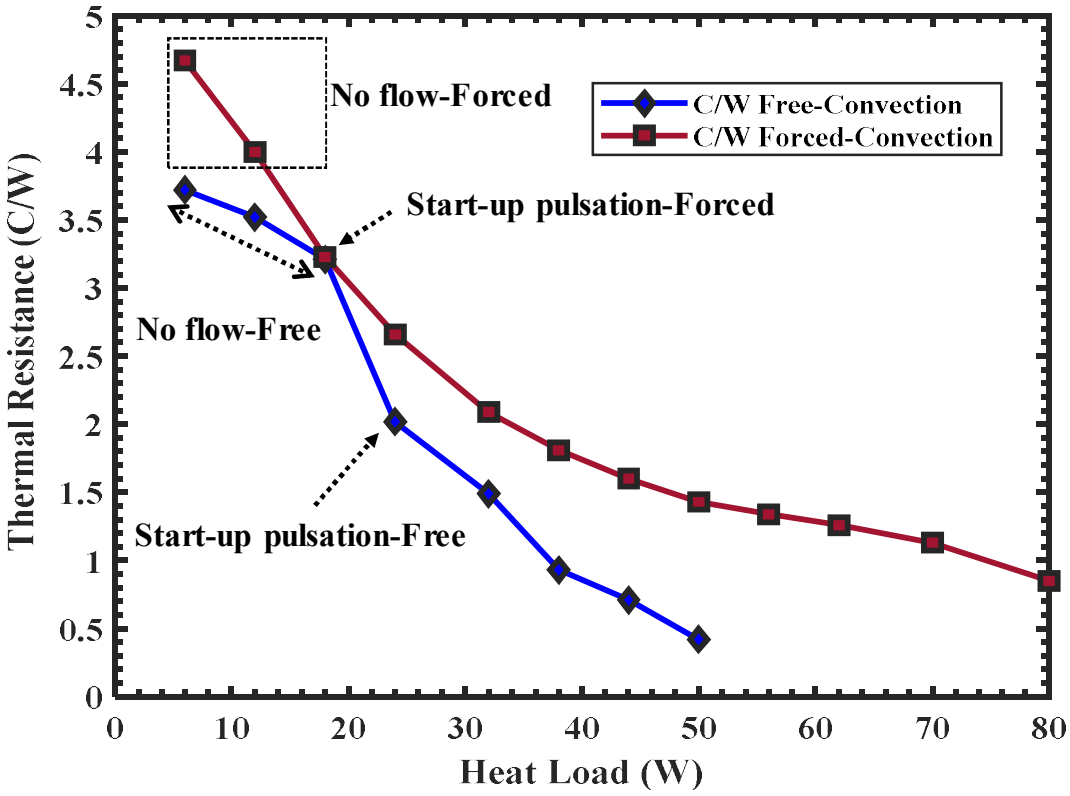

Fig 3.4. Comparison of thermal resistance for free and forced convective CLPHP.

Figure 3.5(a) represents the value of h_{eff} calculated by Eq. (13). The blue and red curves are the transfer coefficients of forced and free convection, respectively. The h_{eff} value rapidly increases with the increase in Q_{in} until the system reaches an initial dry-out condition, where h_{eff} drops suddenly. h_{eff} is higher for the free convective CLPHP owing to the significant density variations of the working fluid, which changes because of the temperature variations in fluid. The density of the working fluid changes in the boundary layer during evaporation, which causes the fluid to rise. Then, it is replaced by the cool working fluid, which also increases owing to heating. This phenomenon continues until the fluid reaches the initial dry-out conditions, which leads to the higher heat transfer rate of the evaporator section between

start-up pulsations and dry-out.

Figure 3.5(b) shows the K_{eff} of free and forced convective CLPHP derived from Eq. (12). K_{eff} increases with the increase in Q_{in} for both free and forced convection. The small L_{tot} (20 mm) through natural convection for the current set-up leads to a lower K_{eff} compared to the forced convective CLPHP. However, for the current experiments, the value of K_{eff} for both free and forced convection is much higher than that of an ordinary glass tube (0.8 W/mK).

Figure 3.5(c) shows the axial and radial heat fluxes for both free and forced convective CLPHP. The CHF is higher for the forced convective CLPHP. In addition, CHF can be further enhanced by providing a greater number of U-bends or U-turns, which can reduce the possibility of stopover phenomena. Further, the fluid has more space to move from one channel to another, but the thermophysical properties of the working fluid must be considered as a rule of thumb.

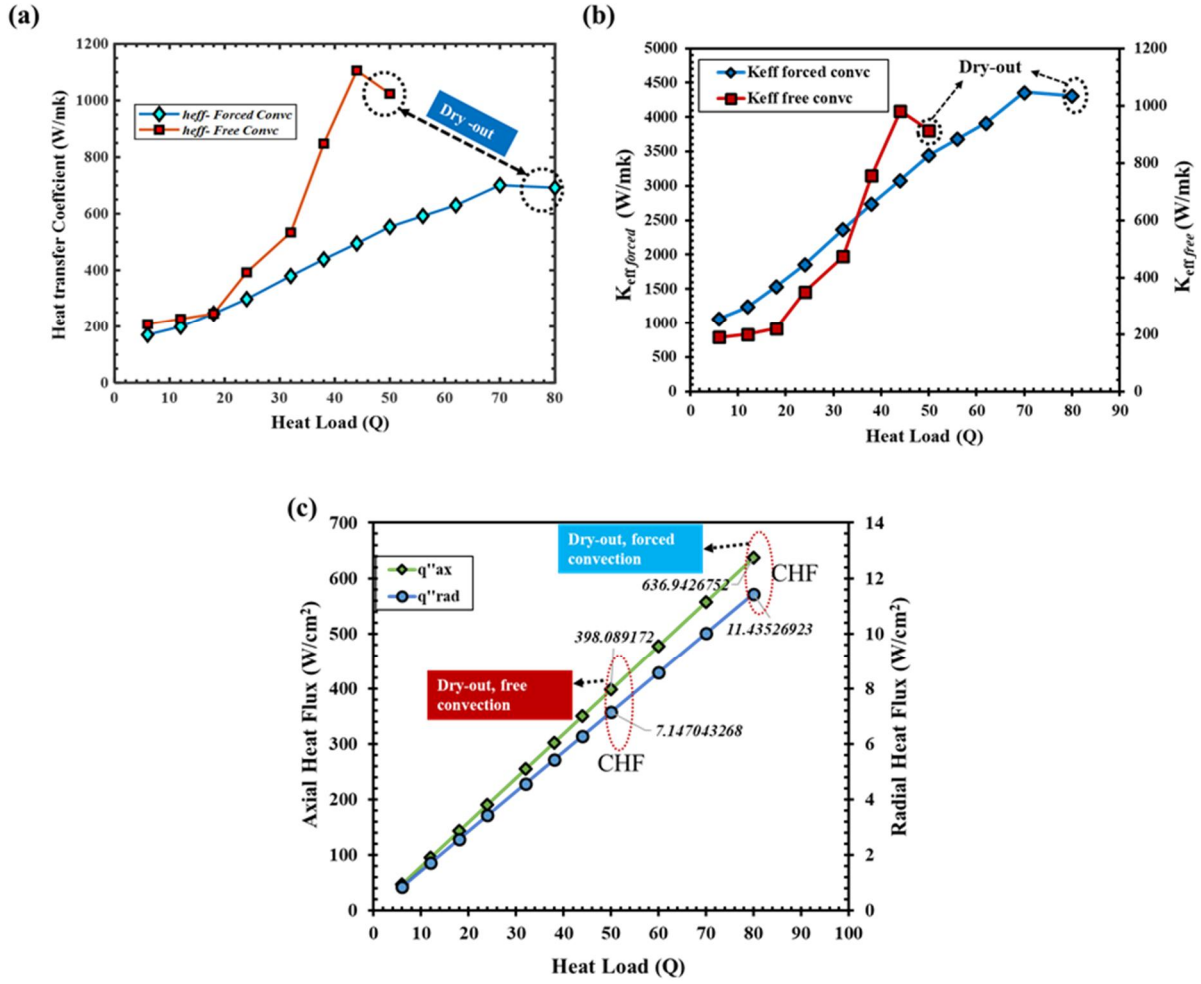

Fig 3.5. Heat transfer characteristics at various Qin. (a) Evaporator heat transfer coefficient, (b) effective thermal conductivity, and (c) axial and radial heat flux.

3.1.4. Flow Visualization

As the heat transfer characteristics depend on the internal flows, a flow visualization technique is used to fully understand the flow behavior inside the capillaries, and to identify the reasons for the heat transfer or heat transfer enhancement through free and forced convective CLPHP. The focus is to capture the dominant, common, and dissimilar flow patterns due to which the performance can be differentiated.

3.1.4.1. Flow behaviors in free convective CLPHP

The flow behaviors are identified by the start-up pulsations and steady-state oscillations in CLPHP. The start-up flow behaviors were experimentally examined by Tong et al. [26]. When the fluid is injected into CLPHP, it distributes randomly into larger vapor plugs (VPs) and liquid slugs (LSs). During free convective CLPHP, when the uniform Q_{in} reaches 24 W (q''_{ax} = 191 W/cm^2, q''_{rad} =3.42 W/cm^2), the pressure in each tube increases by bubble nucleation, which causes the bubble to rise from the evaporator section; thus, start-up pulsation occurs. Figure 3.6(a) shows the typical flow patterns in free convective CLPHP during start-up pulsations. The coalescence of VPs and the generation of LSs along with small bubbles rising from the evaporator section are the dominant flow. The arrows indicate the direction of flows. The oscillations of a bubble are stronger because there is no assisted cooling source to force the bubbles, and thus, the bubble travels a sufficient distance in spite of low Q_{in}.

As the heat further increases to a Q_{in} value of 32 W, the flow patterns change owing to the internal pressure, which distributes the flow into dispersed bubbles, elongated, bubbly, and plug flow in alternative particular channels, as shown in Fig. 3.6(b). A VP merging in the condenser section can also be seen on channel 3 in Fig. 3.6(c). During cases with low Q_{in} for the natural convection, the rate of generation of bubbles from the heating section is higher, which moves to the condenser section in irregular patterns, and a new bubble takes its place in the evaporator section.

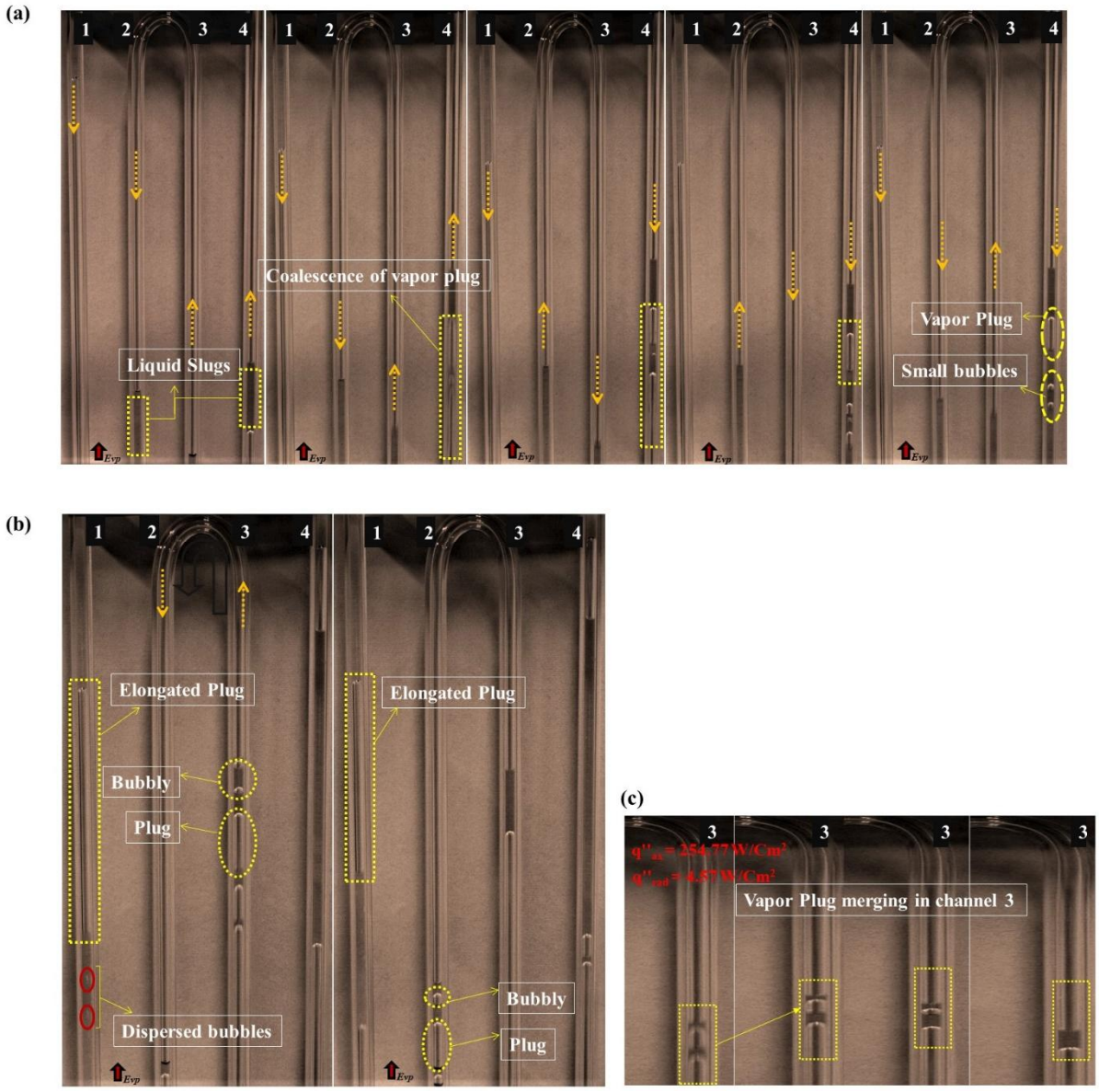

Fig. 3.6. Typical flow behaviors for free convective CLPHP during (a) Start-up Pulsations, (b) Q_{in} of 32 W, and (c) vapor plug merging at a Q_{in} value of 32 W.

When a uniform heat flux increases or the heating time increases for a Q_{in} value of 32 W, interesting flow patterns were observed, as shown in Fig. 3.7(a). When the Q_{in} reaches 32 W, although the flow patterns are still in pulsation mode, the oscillations become faster and the flow direction switches continuously. Within a certain time, each channel has an annular flow, while in other channels, the transition flow occurs by vapor plug train, deformed plug, and bubbly plug. The amount of heat transfer tends to increase owing to the annular

flow and transition of flow patterns. With a small increment in the heat flux, the flow directions suddenly change, and a uni-directional circulation of annular flows, VPs, and LSs were observed for a Q_{in} of 44 W. This is the high heat transfer state because the oscillations of VPs and LSs with a very small intensity are recovered, and any two-neighboring tube has the inverse flow direction, as shown in Fig. 3.7(b). The uni-directional circulation does not last long owing to its faster oscillation recovery, which is changed into a fully developed annular flow in all channels, as shown in Fig. 3.7(c). Further increasing the heat leads to the channels dry-patch, and there is, therefore, insufficient fluid in the tubes to transfer heat in the channels. Therefore, the heat to the system was stopped, and thus this stage was considered as the CHF for the free convective CLPHP. The dry-out evaporator section is not shown in this study because the evaporator section was insulated, and it is difficult to capture that section. However, the dry-out evaporator section can be predicted by the sharp rise in T_e at high Q_{in}.

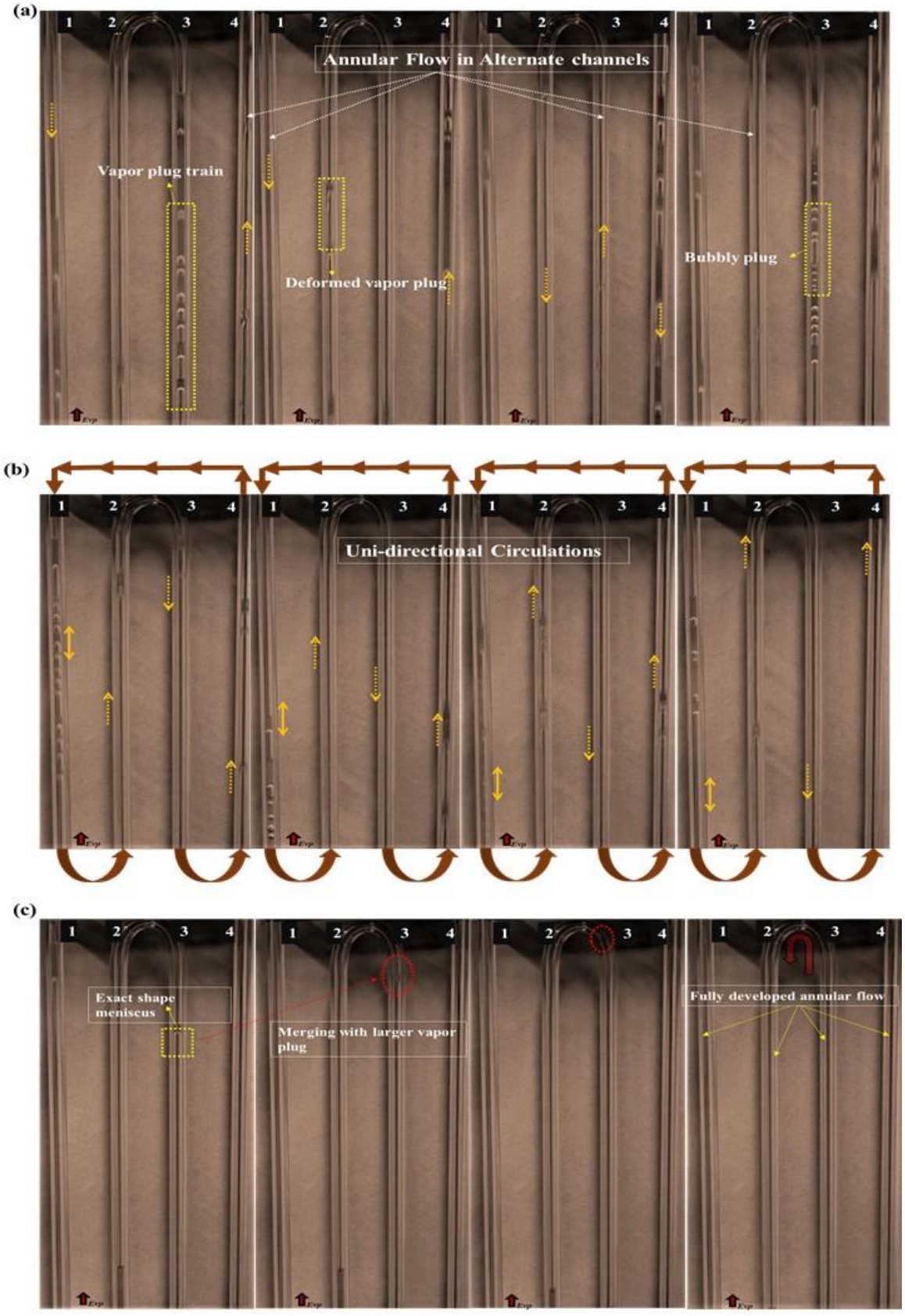

Fig. 3.7. Flow behaviors for Q_{in} values of (a) 32 W, (b) 44 W (unidirectional circulations),

and (c) 44 W (annular flow).

3.1.4.2. Flow behaviors in forced convective CLPHP

A similar study was performed for forced convective CLPHP. The sequence of the flow phenomena inside the tubes is slightly different from that of the free convective CLPHP owing to the assisted DC fan, which plays a vital role in the phase change. As the initial pulsations occurred early at a Q_{in} value of 18 W, when the driven force from the evaporator section was too low, the oscillations of these bubbles were limited to its specific channels. These oscillations can be understood from the displacement of the bubbles discussed in Section 3.5. Figure 3.8(a) shows the bubble oscillation during start-up pulsation for 0.2 s. This oscillation is limited until the heat flux was gradually increased to a Q_{in} value of 24 W during the entire period, where the two-phase working fluid formed into the VP and LS train along the entire tube. These heat flux conditions made it possible for the VPs and LSs to be altered in the U-shaped section of the evaporator. After further increasing the heat flux, which increases the evaporator temperature with a balanced condensing force, the dominant flow was the formation of new LSs and VPs merging with the elongated flow.

An interesting flow was observed at a Q_{in} value of 38 W, where the heat flux increases the internal fluid pressure, which arranges the flow into inertial dominated and gravitational dominated flow, as shown in Fig. 3.8(b). The arrows represent the flow direction during a particular time. The inertial dominated flow moves upwards in channel 4 to the upper U-bend owing to the strongly driven conditions from the evaporator section. Therefore, a quick restoring force from the condenser arranges this flow into a gravitational dominated downward flow along with the deformed plug flow and dispersed bubbles in the alternative channels, as indicated in Fig. 3.8(b). These flows are constantly generated and break into deformed plug

flows.

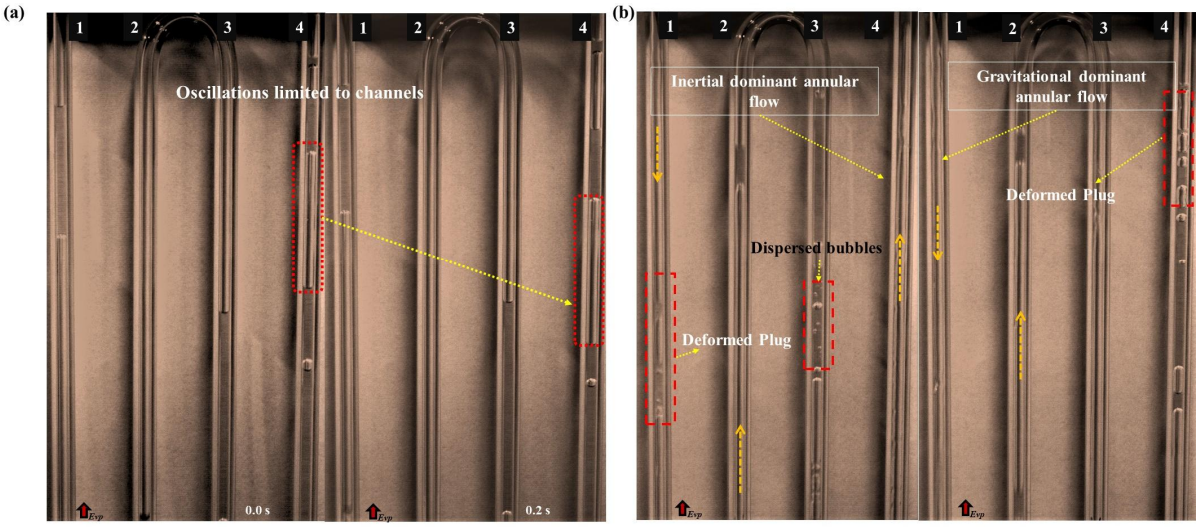

Fig. 3.8. Flow patterns at Q_{in} of (a) 18 W (Start-up pulsations) and (b) 38 W.

When the value of Q_{in} was increased from 38 W to 44 W, a transition flow with a liquid ring was observed in channel 4, as shown in Fig. 3.9(a). The liquid ring transition flow was the dominant flow pattern at this stage. A liquid ring from the evaporator to the condenser section is observed, and progresses with an annular flow at the adiabatic section, whereas the condenser U-bend section was active in the attachment of bubbles, as indicated in Fig. 3.9(b). The bubble usually appears before the U-bend condenser section, semi-attached in the U-bend section, while it is fully attached after the U-bend, which is then moved to the evaporator section and a new bubble takes its place, and vice versa. When the Q_{in} is increased to 50 W, the exact shape of the meniscus heads was observed as shown in Fig. 3.9(c).

The heat transfer enhancement by the meniscus head in PHPs is briefly discussed in a previous study by Sole-Agostineli et al. [28]. These meniscus heads enhance the heat transfer rate because of their higher amplitude oscillations. A transition flow with a liquid bridge to annular flow was also observed at this stage, as shown in Fig. 3.9(c).

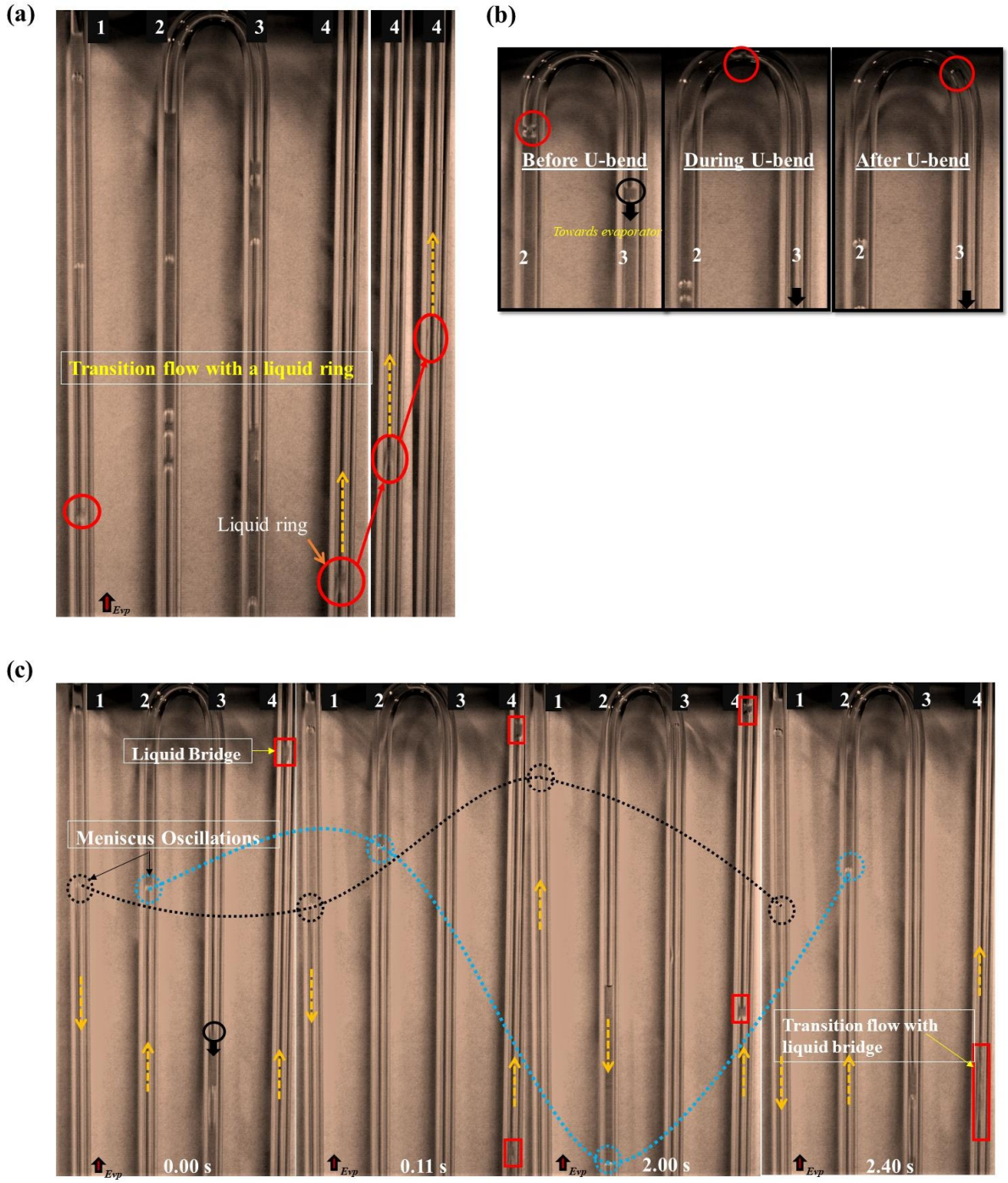

Fig 3.9. (a) Transitions flow with the liquid ring at a Q_{in} value of 44 W, (b) Bubble attachment phenomena before, during, and after the U-bend at a Q_{in} value of 44 W, and (c) meniscus head oscillations/pulsations at a Q_{in} value of 50 W.

The liquid thin films (LTFs) tend to appear as Q_{in} further increases to 62 W because of the drastic increase in T_e. Increasing Q_{in} above 50 W leads to a high aggregate of the LTFs

in the tubes. A typical LTF in a particular channel was selected, and a three-step image segmentation was done in order to fully visualize the LTF for the considered frame. Image J and MATLAB were used to perform enhancing, masking, and thresholding of the image. The images were enhanced by a contrasting function in Image J, and masking and thresholding were done by the image segmenter and color thresholder function in MATLAB. The typical image segmentation of LTF in a particular channel is shown in Fig. 3.10(a). The blue area represents the LTF, whereas the white area represents a VP. A uni-directional circulation recovering the VPs and LSs was observed at a Q_{in} value of 70 W, as shown in Fig. 3.10(b). The amount of heat transfer increases because of a sharp recovery of VPs and LSs. Owing to the uni-directional circulation and high heat rejection rate, the circulations rapidly develop to an annular flow. When T_e increases, the internal flow between the hot and cold sources arranges itself differently, and only annular flow can occur inside the tubes with circulations in one direction [57]. The dry patch tends to appear from this stage, and further increasing Q_{in} leads to the CHF state, which can be identified by the unexpected rise in the T_e.

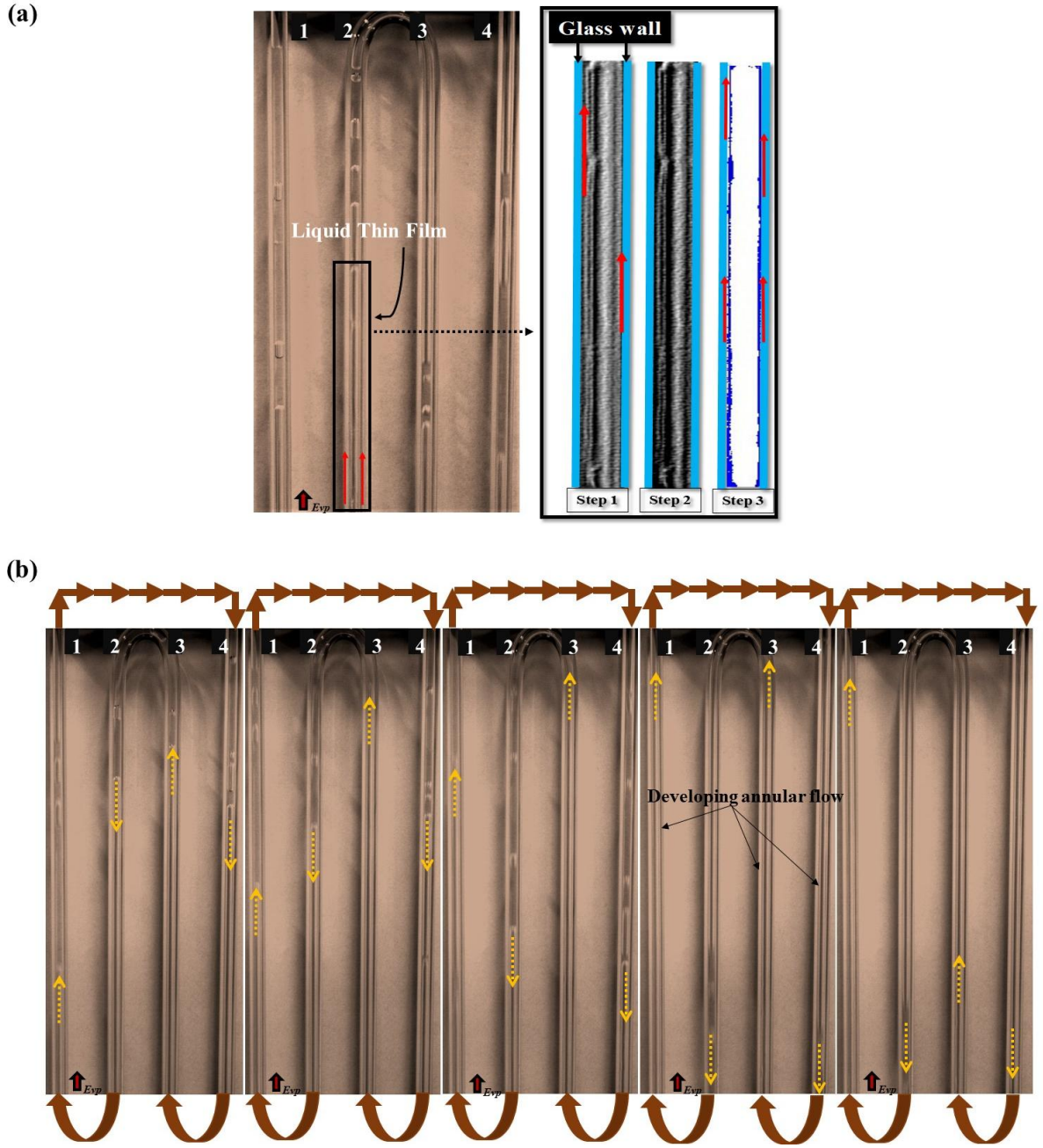

Fig 3.10. (a) Liquid thin-film (LTF) observation through three-step image segmentation and (b) Uni-directional oscillatory developed annular flow patterns.

From the sequences of all the flow regimes inside the tube, it can be concluded that the internal flow regimes from start-up to dry-out patch are strongly dependent on the Q_{in}, cooling source, thermophysical properties of the working fluid, internal diameter, etc. When a device achieves a fully developed annular flow with circulations in one direction, a further

increase in Q_{in} causes a longer or fully dry-out state because the bubble velocity increases with the increase in T_e compared to that of the critical value. Figure 3.11 (a-b) illustrates the changes in the flow states of the working fluid in the tubes when Q_{in} increases for both free and forced convection respectively.

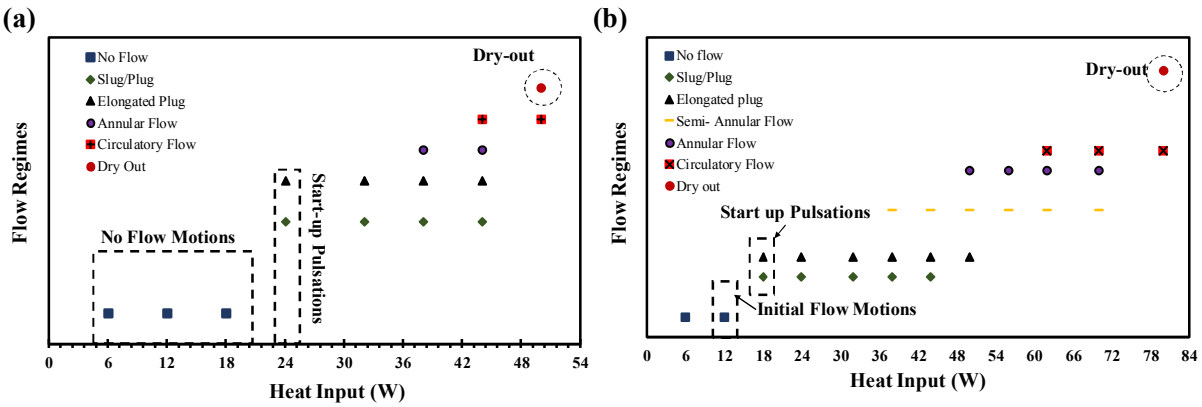

Fig 3.11. States of flow changes from start-up pulsations to dry-out conditions for (a) free and (b) Forced convection.

3.1.5. Bubble displacement, velocity, and acceleration

The bubble displacement, velocity, and acceleration are examined for various values of Q_{in}. The normalized bubble displacement is defined as the ratio of the bubble displacement in the visual section to the total length of the visual section (a visual length of 151 mm was selected and consisted of adiabatic and condenser sections). For free convective CLPHP operation, the bubble displacements and velocities during start-up and normal operating mode are represented in Figs. 3.12(a-f). A sudden start-up of bubble oscillations can also be understood from the bubble displacement and its velocities, as indicated in Figs. 3.12(a-b). The velocity of the bubbles varies for each section, as shown in Fig. 3.12(b). The positive velocity indicates the upward motion of the bubble, whereas the negative velocity refers to the downward motion. During start-up pulsations, some of the bubbles move downward to the evaporator section,

which moves toward the condenser section after heating. Although some bubbles have a higher velocity owing to its own displacement in the channel, the mean velocity lies in the range of 0.01 m/s to 0.15 m/s.

For a Q_{in} value of 32 W, the oscillations become active, which also increases the velocity in each channel, as shown in Figs. 3.12(c-d). The amplitude of the oscillations increases in each channel, which increases the velocities. The displacement and velocity for each channel are different as with start-up pulsations. The mean velocity is increased owing to the amplitude of the irregular oscillations. One can see that the velocity of some channels reaches 0.8 m/s. However, the mean velocity of the channels lies within the range of 0.1 m/s to 0.25 m/s.

For a higher Q_{in} (44 W) in free convective CLPHP, as the dominant flow is the annular flow, it is difficult to track the bubble because its head does not appear in the visual screen for a long duration. However, the trackers were set near the evaporator section, and the displacement was measured when the head of the bubbles appears on the visual screen. Its amplitude is greater than 151 mm for channels 1 and 4. For channels 2 and 3, although the amplitude of the bubble heads was dependent on the flow pattern (slug/plug flows, circulations, and annular flows) because there was a transition flow, the amplitude of the bubbles is large during the upward movement, as shown in Fig. 3.12(e). This stage was considered to be the higher bubble velocity phase, as shown in Fig. 3.12(f), owing to a sharp increase in T_e, rapid bubble motion, and flow crossover in uni-directional circulations. The slope of the velocity of channels varies for each channel because of the internal flow motions. The average velocity of the channels is increased from 0.25 m/s to 1.54 m/s.

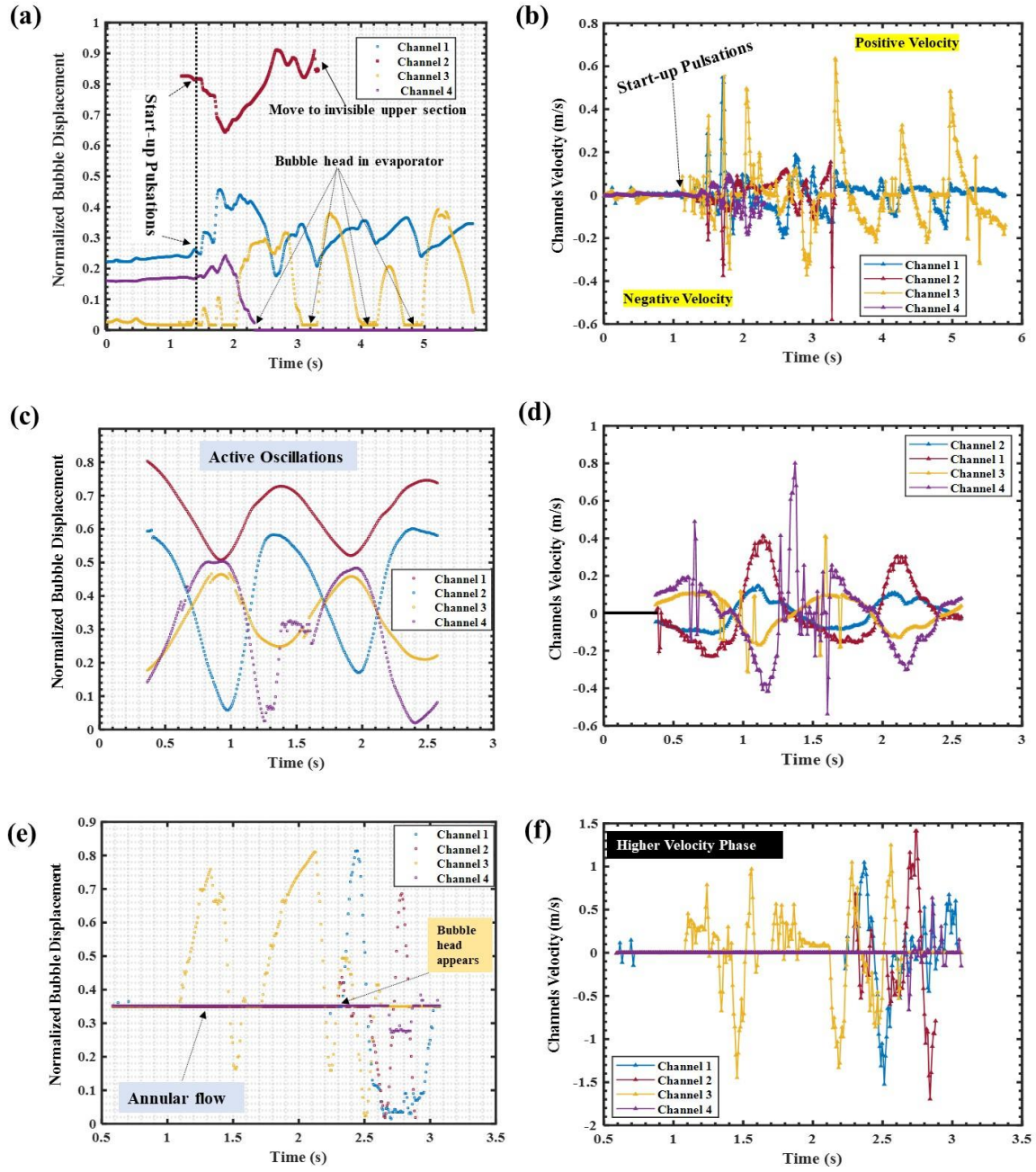

Fig 3.12. Bubble displacements and velocities at the Q_{in} of (a-b) 24 W (start-up pulsations), (c-d) 32 W, and (e-f) 44 W for natural convective CLPHP.

Figure 3.13 shows the bubble displacements and velocities for forced convective CLPHP for start-up pulsations for a Q_{in} value up to 50 W. It is interesting to observe that during start-up pulsations, the oscillations are vigorous besides they are restrained to its particular. A clear 90º phase can be seen from the velocity distributions, as shown in Fig. 3.13(b). The amplitudes of both positive upward and negative downward velocities are within the range of

0.1 m/s to - 0.1 m/s. The mean velocity is 0.075 m/s. For a Q_{in} value of 32 W, the oscillations become random owing to an increase in T_e and T_c, which maintains a balanced force between the evaporator and condenser. When Q_{in} reaches 44 W, a rapid bubble motion was observed with the crossover of bulk circulations (i.e., either clockwise or anti-clockwise circulations). Bubble displacement is an alternative in each channel, and the mean velocity is increased at this stage from 0.075 to 0.1 m/s. Oscillations with meniscus head having an exact shape were dominant, as discussed in the flow visualization section. Therefore, the displacement and velocity of those meniscus heads were measured for a Q_{in} value of 50 W, as shown in Figs. 3.13(g-h). The oscillations of these meniscus heads are marginal, and a significant amplitude is observed during this state. The heat transfer rate is greater at this stage because the velocity of these bubbles increases and the bubble oscillates with a mean velocity of 0.2 m/s.

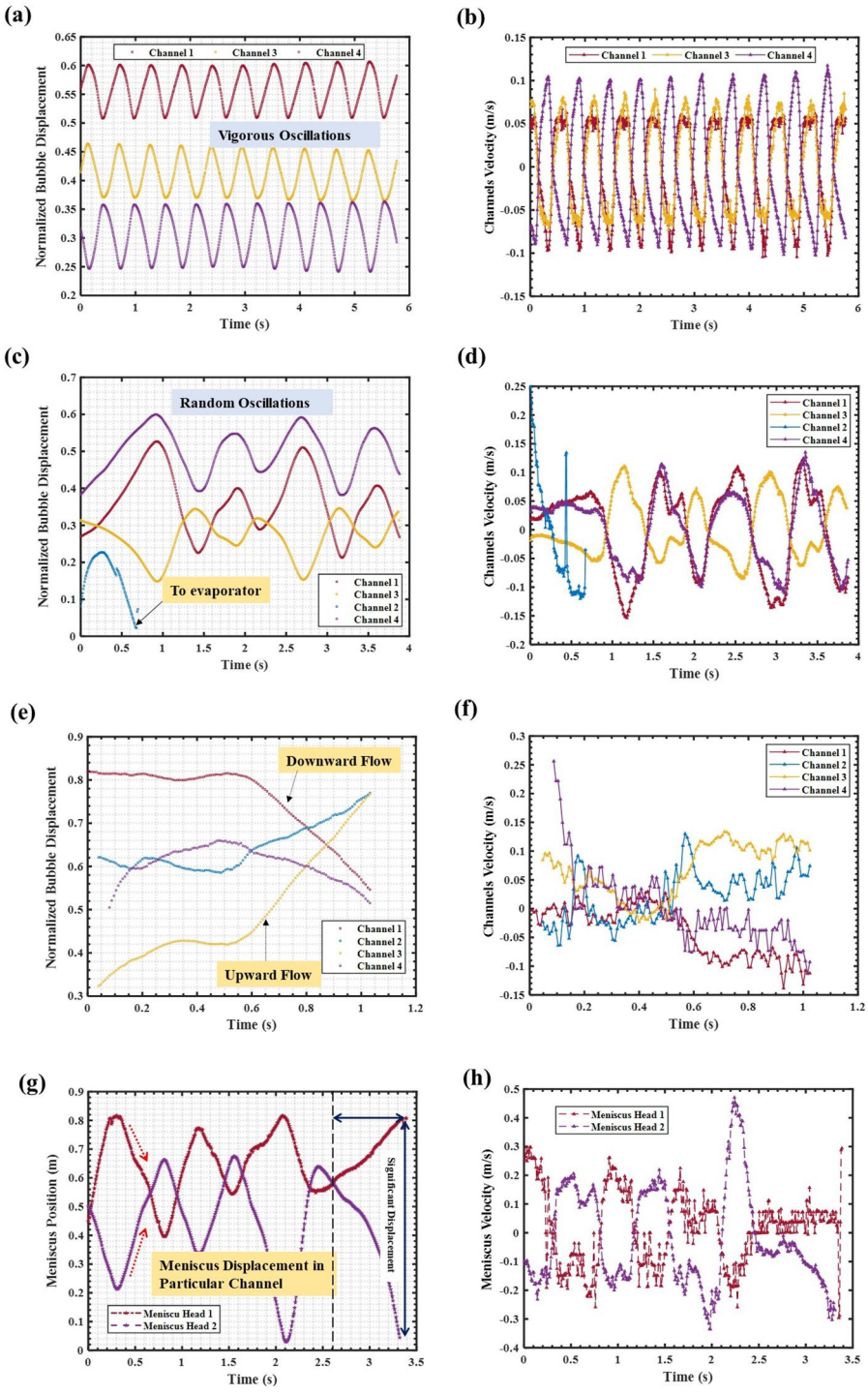

Fig 3.13. Bubble displacement and velocity at Q_{in} of (a-b) 18 W, (c-d) 32 W, (e-f) 44 W (g-h), and 50 W (meniscus head oscillations) for forced convective CLPHP.

For a Q_{in} value of 62 W, the LTF evaporation rate between the wall and bubbles is high, which significantly enhances the heat transfer. At this stage, both the bubble length and the

amplitude of oscillations are increased owing to the intensity of bubble expansion with high velocity [45]. A similar maximum number of pulsations/oscillations were observed in the same way as free convective CLPHP, for which the amplitude was found to be more than the visual section (> 151 mm). Therefore, the bubble displacement was measured for a short duration when the inertial force breaks the LS through a high vapor bubble pressure. At this stage, a rapid bubble displacement from the condenser to evaporator, and vice versa, was observed, which then transforms the flow to annular and semi-annular flow. The displacement and mean average velocity during that time are shown in Figs. 214(a-d) for Q_{in} of 62 W and 70 W. The mean velocity is increased from 0.28 m/s to 0.49 m/s over a time period of 0.5 s to 0.6 s.

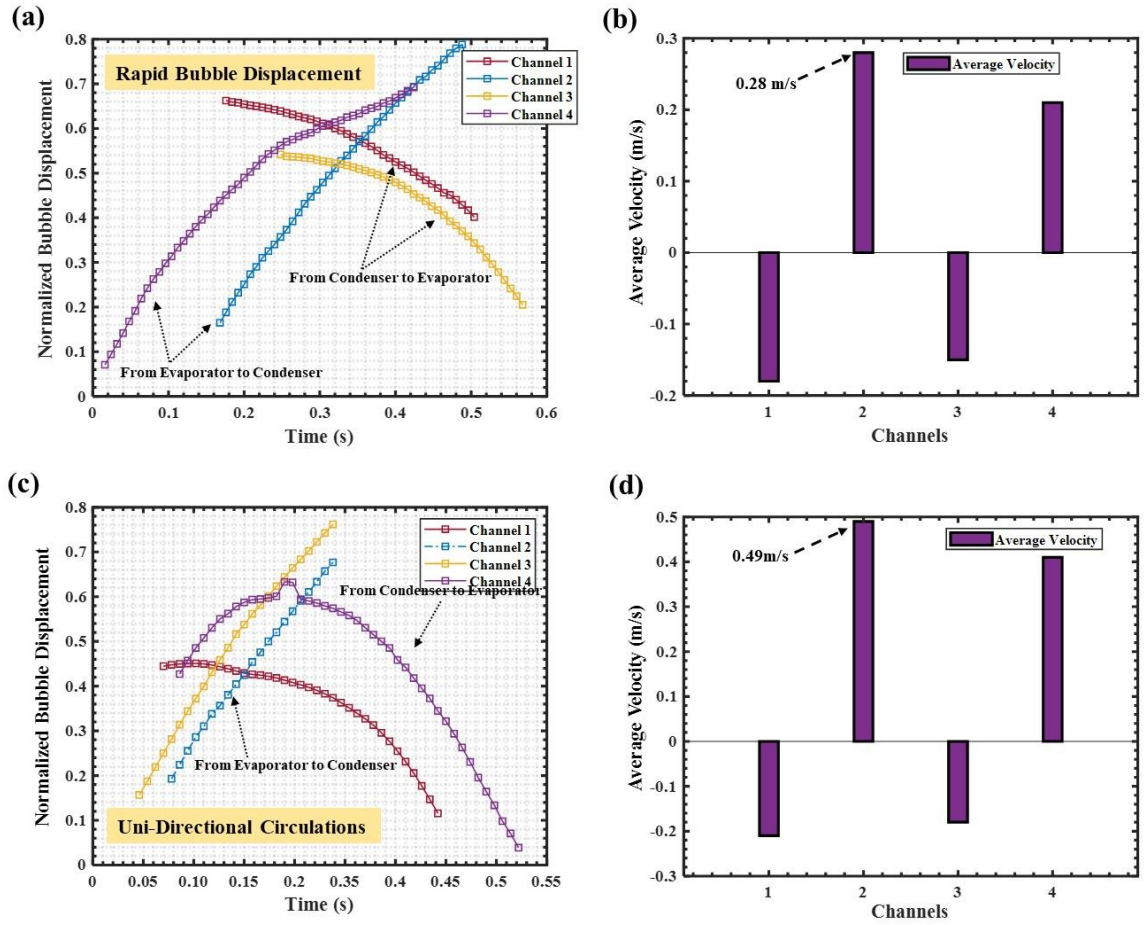

Fig 3.14. Bubble displacement and velocity at Q_{in} (a-b) 62 W and (c-d) 70 W for forced convective CLPHP.

The average bubble acceleration for both free and forced convection CLPHP is shown in Fig. 3.15. The conspired graph reveals the bubble accelerations during different phases as indicated. The acceleration for both upward and downward channel movement is considered as positive. The mean acceleration increases with an increase in Q_{in}. The external source keeps the bubble movements alive for a longer duration, and the mean acceleration of the bubble is higher for forced convective CLPHP owing to the condensation rate.

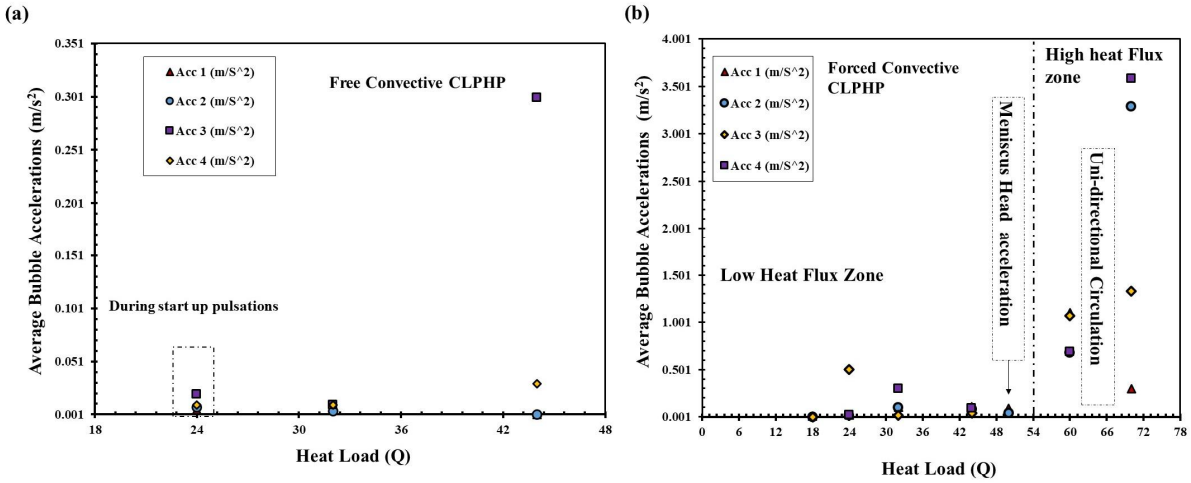

Fig 3.15. Average bubble acceleration at various Q_{in} for (a) free convective and (b) forced convective CLPHP operations.

Table 3.1. demonstrates the changes in the velocity, displacement, and acceleration when Qin increases for both free and forced convection. All values have been taken as the mean values.

Table 3.1. Mean velocity, displacement, and acceleration of free and forced convection concerning Q_{in}.

Free convection				Forced Convection			
Q_{in} (W)	Velocity (m/s)	Acceleration (m/s^2)	Displacement (normalized)	Q_{in} (W)	Velocity (m/s)	Acceleration (m/s^2)	Displacement (normalized)
24	0.01	0.005	0.26	18	0.07	0.001	0.45
32	0.10	0.009	0.32	32	0.05	0.099	0.20
44	1.54	0.160	0.46	44	0.10	0.080	0.54
50	Dry-out	Dry out	Dry out	50	0.20	0.090	0.45
				62	0.28	0.80	0.56
				70	0.49	1.33	0.65
				80	Dry out	Dry out	Dry out

3.2. Experiment 2 (Analysis of thermally driven flow behaviors in ambient conditions).

In this experiment, the manufactured CLPHP is tested under ambient environmental conditions, mounted in the bottom heat vertical mode position, and charged with various filling ratios (FRs), using ethanol as a working fluid. The overall length of the device is 210 mm, the length of the evaporator section is 50 mm, and the remainder of the device consists of the condenser section, which is fully exposed to the ambient room temperature. A series of experiments are performed to investigate the thermal performance and observe the corresponding flow patterns. In this study, an optimal FR ratio of the ethanol is demonstrated and then the visual study is performed to observe the flow dynamics under that optimal FR. The present experimental approach facilitates the design of a glass-tube CLPHP that operates under ambient conditions when ethanol is used as a working fluid with its certain FR. The results obtained from this study are as follows,

3.2.1. Temperature distributions and thermal-performance observations

The thermal performance was evaluated using the R_{th} of the GT-CLPHP, as defined in Equation (5). The overall R_{th} values for the FRs of 20%, 30%, 40%, 50%, and 60% are shown in Fig. 3.16. First, the Q_{in} for each experiment was gradually increased with the interval of 10 W between Q_{in} for all FRs. As shown in Fig. 24, the device yielded a superior and more acceptable R_{th} for the 50% FR. Therefore, a separate experiment was performed for the FR of 50% by gradually increasing the Q_{in} at the interval of 5 W between Q_{in} to investigate the flow behaviors inside the CLPHP, because the thermal performance was significantly dependent

on the flow motion and phase change inside the CLPHP.

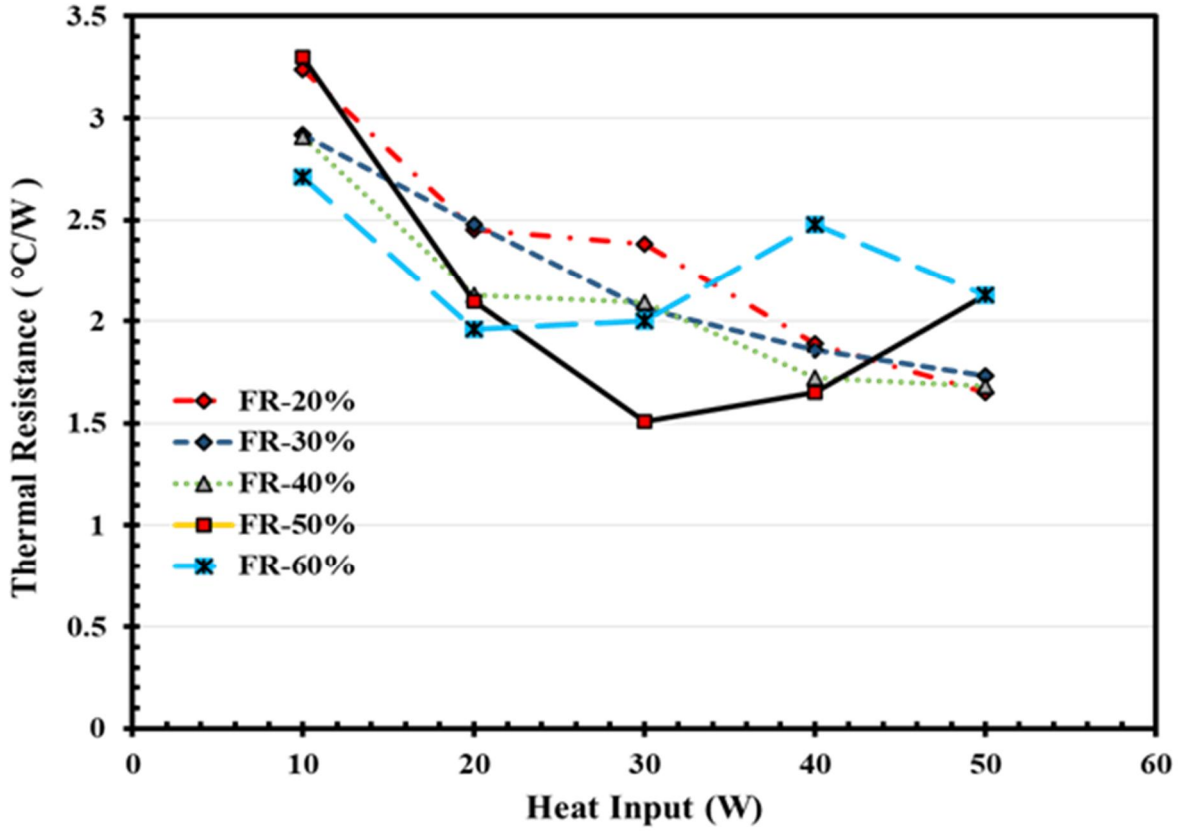

Fig 3.16. Thermal-resistance variations for various FRs.

As shown in Fig. 3.16, the R_{th} of the CLPHP decreased with the increase of Q_{in} for the FRs of 20%, 30%, 40%, and 50%. The performance of the CLPHP in terms of R_{th} is different for the FR of 60%. For the 60% FR, the R_{th} decreased when Q_{in} increased up to 20 W, and then it rises with higher Q_{in}. At lower Q_{in} i.e., 10 W and 20 W, the 60% FR yielded better performance than the other FRs, but the performance became poor with a further increase in Q_{in}. For a 40% FR with a high Q_{in}, the thermal performance was most likely stable, but there was no notable enhancement in R_{th} overall. Interestingly, no dry-out occurred for any of the FR and Q_{in} values tested in our experimental study.

The most stable performance was achieved with an FR of 50%. As shown in Fig. 3.16, R_{th} decreased significantly (from 3.30 to 1.65 ℃/W) as Q_{in} increased from 10 to 40 W. This was

due to the presence of a prime flow regime inside the GT-CLPHP, which oscillated with a larger amplitude at a higher Q_{in}. However, at 50W, the dry-out condition leads to increase in R_{th}. The lowest R_{th} was observed for the 50% FR at a high Q_{in}, yielding an optimal FR for the current design. Therefore, further flow regimes inside the channels were investigated at this FR.

The T_{evap} and T_{cond} distributions for FRs of 20%, 30%, 40%, 50%, and 60% are shown in Figs. 3.17(a)–(e), respectively. Both temperature distributions increased with the increase of Q_{in}. Most interestingly, the initial flow motions had various flow patterns at the same $T_{evap,}$ and the quasi-steady state can be confirmed by T_{evap}. For all the FRs, T_{evap} commonly increased with Q_{in}, which is consistent with the tendency observed in previous studies by Ma et al. [47]. For the 20% FR, T_{evap} increased significantly as Q_{in} increased. There were no specific changes in R_{th}, although the initial flow motion was observed at a Q_{in} of 20 W with an R_{th} of 2.89 ℃/W. Throughout the experiments, the 20% FR was poor with regard to thermal performance and flow motions.

As the FR increased from 20% to 30%, changes occurred in the thermal performance and flow motion. The initial flow for a 30% FR was also observed at a Q_{in} of 20 W. A small amplitude motion with a very small damping oscillation was observed when Q_{in} was further increased. These oscillations carried small VPs and LSs and intermittent flow, which causes poor motions with a very low velocity.

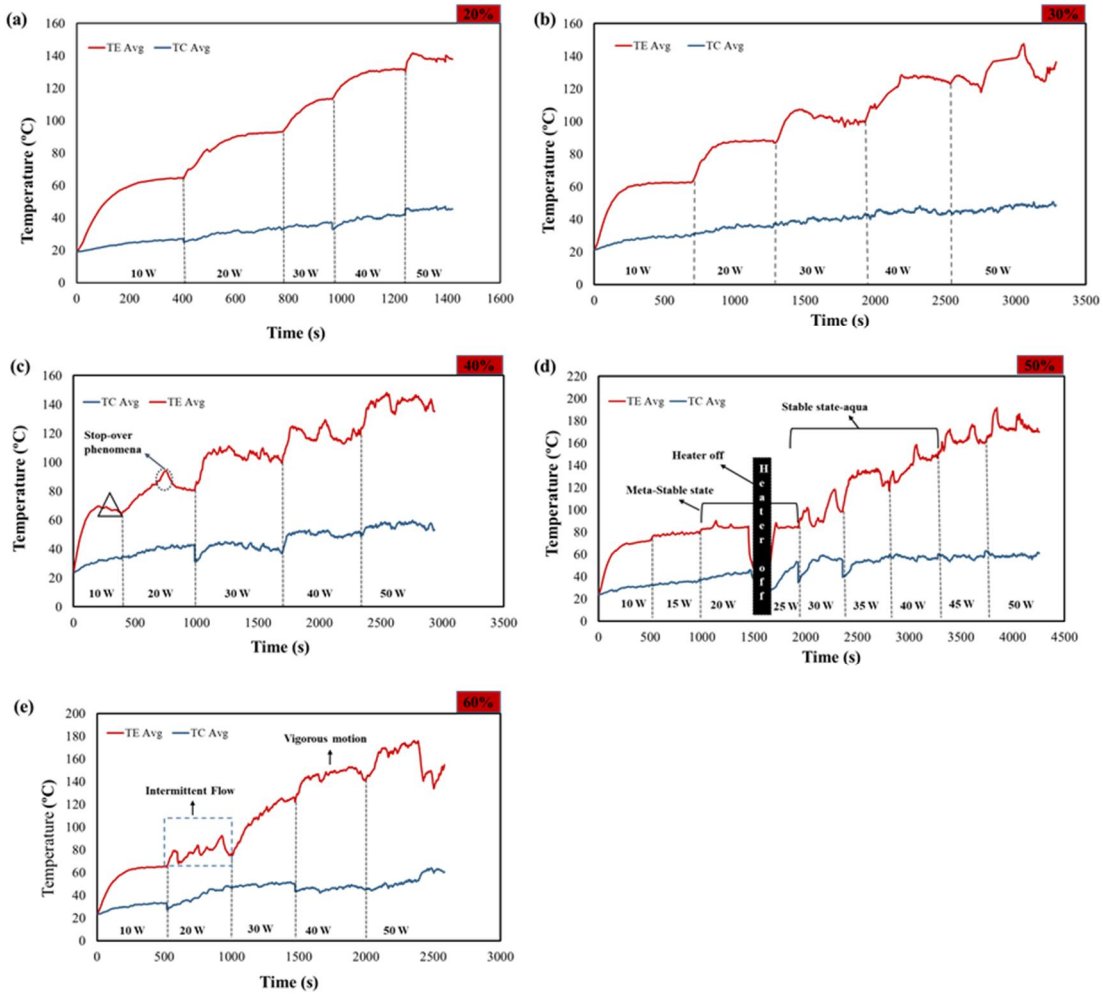

Fig 3.17. Temperature variations in the evaporation section for various Q_{in} values and FRs of (a) 20%, (b) 30%, (c) 40%, (d) 50%, and (e) 60%.

When the FR increased from 30% to 40%, the initial flow motions were observed at a Q_{in} of 10 W, as marked in Fig. 3.17(c) with a triangular shape. As Q_{in} increased, the flow oscillations stopped for a few seconds, causing a decrease in T_{evap}. This was caused by a temporary stoppage of the flow of fluids from the condenser section to the evaporator section in the capillaries. The flow started again after the necessary heat was obtained. As Q_{in} increased further, T_{evap} increased, and some larger VPs appeared. Traveling in a channel with a larger amplitude led to better thermal performance with a higher Q_{in}, i.e., 1.72 ℃/W at 40 W. As Q_{in} increased further (up to 50 W), the oscillations became faster, with an R_{th} of

1.68 ° C/W.

In Fig. 3.17(d), the T_{evap} distributions for the 50% FR with intervals of 5 W between each Q_{in} are presented. T_{evap} increased significantly with an increase in Q_{in}, yielding optimal results for the thermal performance and flow regimes, particularly at a high Q_{in}. The flow phenomena and thermal performance were categorized into the metastable and stable states for Q_{in} values of 20–25 W and 30–40 W, respectively.

For a 60% FR, T_{evap} increased with an increase in Q_{in}, but the overall performance was unsatisfactory. As shown in Fig. 3.17, the performance deteriorated with an increase in Q_{in}, and R_{th} reached 2.13 ℃/W at 50 W. This behavior was induced by the excess volume of fluid inside the channels, which required more energy to balance the inside forces. This caused the flow to be distributed into intermittent conditions. When T_{evap} diminishes at 50 W, the condensed fluid oscillated in the evaporator section. At this time, in the upper section of the condenser, the flow converged, and irregular flow patterns were observed owing to the two-turn device structure.

Fig. 3.18 shows the complex motion analysis of T_{evap} for the 50% FR observed during stable-state behaviors for a short duration at 30, 35, and 40 W. These phenomena can be referred to as chaotic motions, where a small change in temperature leads to a different behavior for the system. The motions have structural similarities to those in Lorenz chaos theory, as minor changes in the Q_{in} can lead to differences in the temperature and flow patterns.

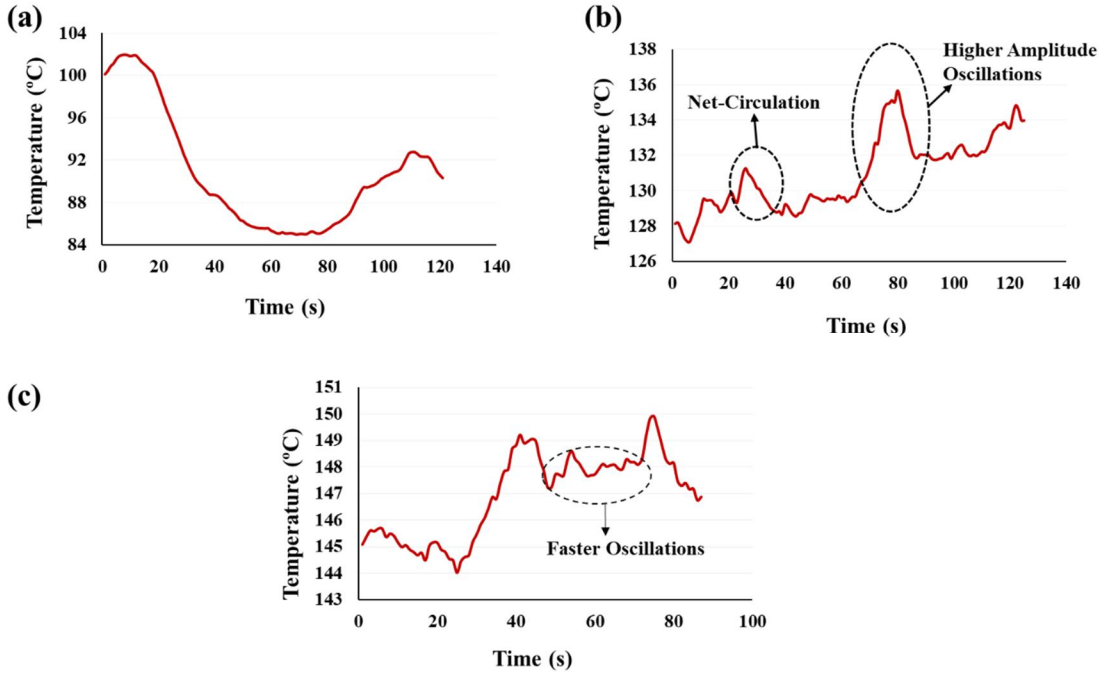

Fig 3.18. Resemblance to Lorenz chaos theory with a 50% FR for complex motions at (a) Q = 30 W for 120 s, (b) Q = 35 W for 130 s, and (c) Q = 40 W for 95 s.

Fig. 3.18(a) shows the amplitude for a 50% FR with a Q_{in} of 30 W during steady-state motions for 130 s. The amplitude of the temperature for 65 s was in the range of 17–18 ℃. In contrast, for the last 65 s, the temperature difference decreased to 4–4.5 ℃. Examining this difference revealed that the initial temperature changed markedly from 102 to 85 ℃ for 65 s, whereas the change in the final temperature was minor (85 to 89.5 ℃), indicating that the chaotic patterns of the initial change were dissimilar to those of the final change for 130 s. This temperature carried the majority of larger VPs and annular VPs (AVPs) in oscillating patterns from the evaporator to the condenser and then back to the evaporator. Fig. 3.18(b) reveals the complex motion for 50% FR at a Q_{in} of 35 W for 130 s. As temperature increased from 30 to 35 W, multiple flow phenomena occurred. This heat load was sufficient to create a circulating two-phase flow. The net circulation barely maintained a temperature difference of 2–2.5 ℃ for 20 s. Larger amplitude oscillations for a long duration maintained a temperature

difference of 6 to 4 ℃. Similarly, Fig. 3.18(c) presents the complex motion behaviors for 40 W. For the initial 25 s, the amplitude of the oscillations was small, leading to a temperature difference of 1.5 ℃. From 25 to 48 s, the amplitude of the initially small oscillations became larger, with a temperature difference of 6 ℃, similar to that at 35 W. Thereafter, faster oscillations along with a circulating two-phase flow were observed for 20 s, with a temperature difference of 2 ℃.

3.2.2. Flow visualization

High-speed imaging was employed for visualizing flows for the 50% FR, which yielded the highest thermal performance. The heat transfer and overall thermal performance of PHPs are strongly influenced by the flow phenomena, and the flow behaviors are generally impacted by the value of Q_{in} [27, 48]. Fig. 3.19(a) presents the initial flow configuration immediately after the injection of the working fluid. It was distributed into LSs, VPs, and small bubbles after filling without any heat load, owing to the dominance of the surface tension over the gravitational acceleration even though the device was vertically mounted. Fig. 3.19(b) shows the flow regimes corresponding to the T_{evap} distribution for 15 and 20 W. Up to a Q_{in} of 15 W, there were no specific changes in the flow motions in the channels for a 50% FR. As the Q_{in} increased from 15 to 20 W, dispersed bubbles appeared. Thereafter, the flow was arranged into larger VPs as the internal velocity of the fluid increased with a larger Q_{in}, as shown in the enlarged view in Fig. 3.19(c).

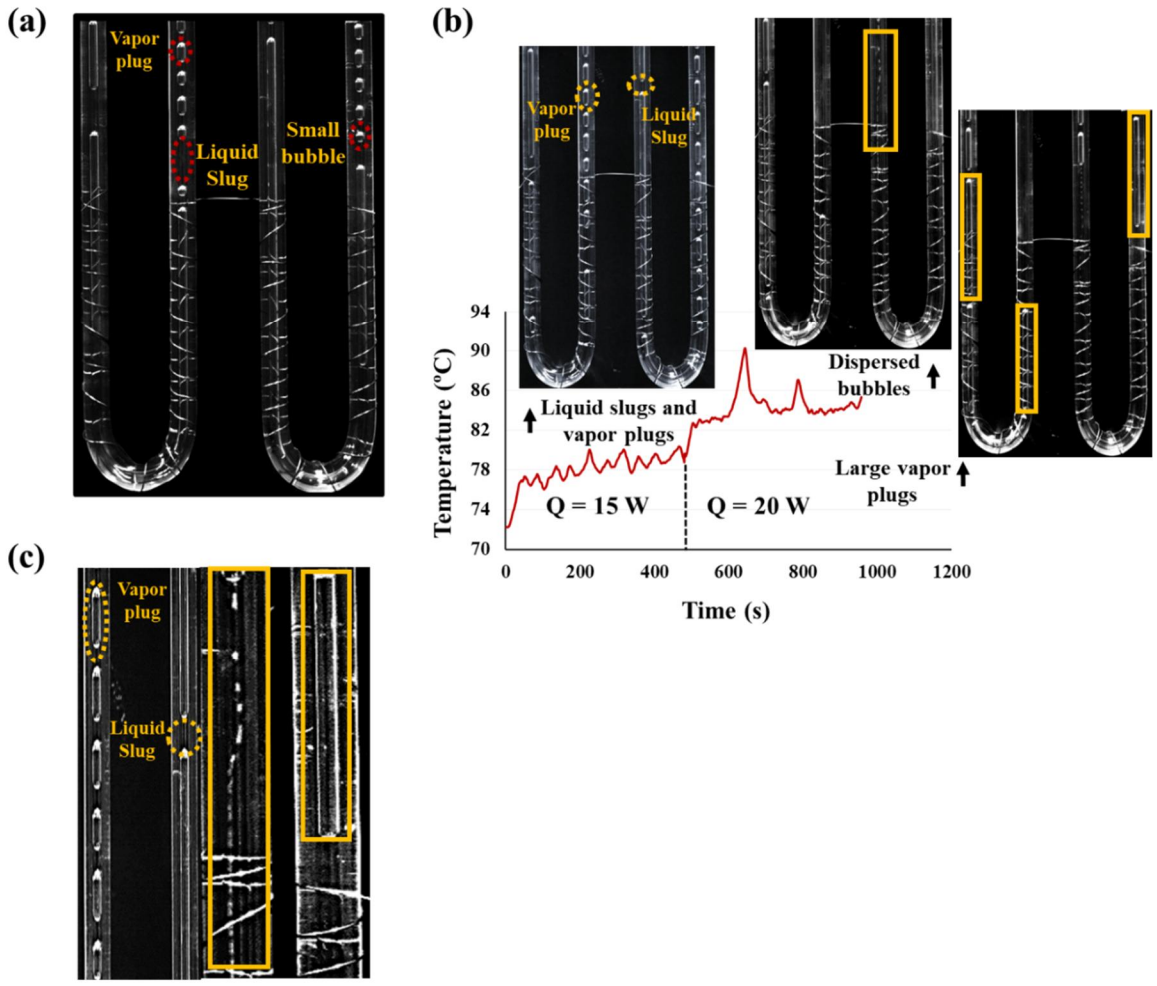

Fig 3.19. Initial flow configurations for 50% FR ethanol (a) immediately after the fluid was injected. (b) Flow patterns at 15 and 20 W. (c) Expanded view of the marked flow in (b).

When Q_{in} increased, the fluid oscillations became powerful because the velocity of the internal fluid altering the flow patterns increased [30]. The majority of the heat was transferred by the sensible heat, and the AVPs were observed at 25 W. At this stage, the small bubbles in the channels merged with others, leading to larger VPs. Simultaneously, the AVP oscillated in the U-shaped evaporator with a very small amplitude. This stage was considered to be the metastable state, as shown in Fig. 3.17(d). In this state, the smaller VPs responsible for the poor flow oscillations transformed into larger VPs. Additionally, the larger VPs transformed into annular and semi-annular VPs, and the flow was alternated in the

channels. With a further increase in Q_{in}, the oscillations of the AVPs increased. At 30 W, the majority of the observed flow was linked to the annular and semi-annular VPs. At a certain time, one of these plugs was wrapped in a thin film, leading to further stable-state flow behavior. The flow was categorized into larger VPs, AVPs, semi-AVPs, and AVP surrounded by a thin film.

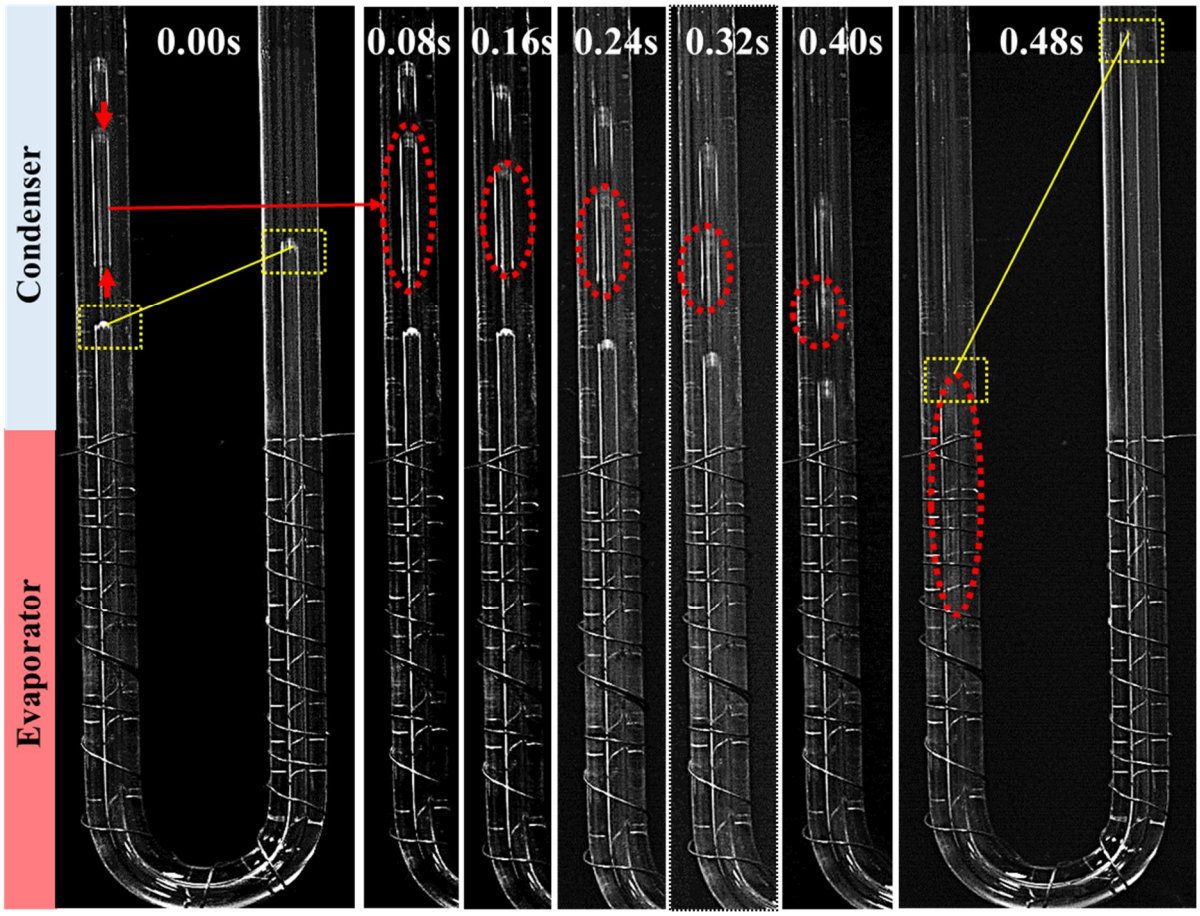

Fig 3.20. Shrinking and elongation of a single VP transferring its energy to the larger VP growing a meniscus head at Q_{in} = 35 W.

The more interesting flow was observed for Q_{in} = 35 W. Fig. 3.20 shows the operation of a single VP capturing energy and transferring its energy to a larger AVP. The VP shrank with a low velocity and captured the energy within itself. Simultaneously, the adjoined larger AVP in the U-shaped channel played the role of the receiver. The energy captured by the VP was then transferred with a higher velocity to the larger AVPs, which helped the larger

AVP to grow its meniscus head with greater amplitude oscillations.

Fig. 3.21 presents a graphical explanation of this phenomenon. The ImageJ software was used to measure the positions of the VPs after image segmentation using the adjusting function of the brightness, contrast, gamma, and exposures in Adobe Photoshop. Thereafter, the overall length was calculated using the two meniscus positions at both ends in one VP. Fig. 3.21(a) shows that the amplitude and velocity of the VP decreased over time in the VP shrinking phase. However, the velocity and amplitude of the VP increased sharply at the time of transferring energy and merging with an AVP. Fig. 3.21(b) represents the overall AVP length before and after the merging of the VP. The larger AVP had an overall amplitude of 159.741 mm before the VP merging. After the merging of the VP, the amplitude reached 172.80 mm, with a velocity of 295.06 mm/s. This larger amplitude stabilized the motions for the oscillations.

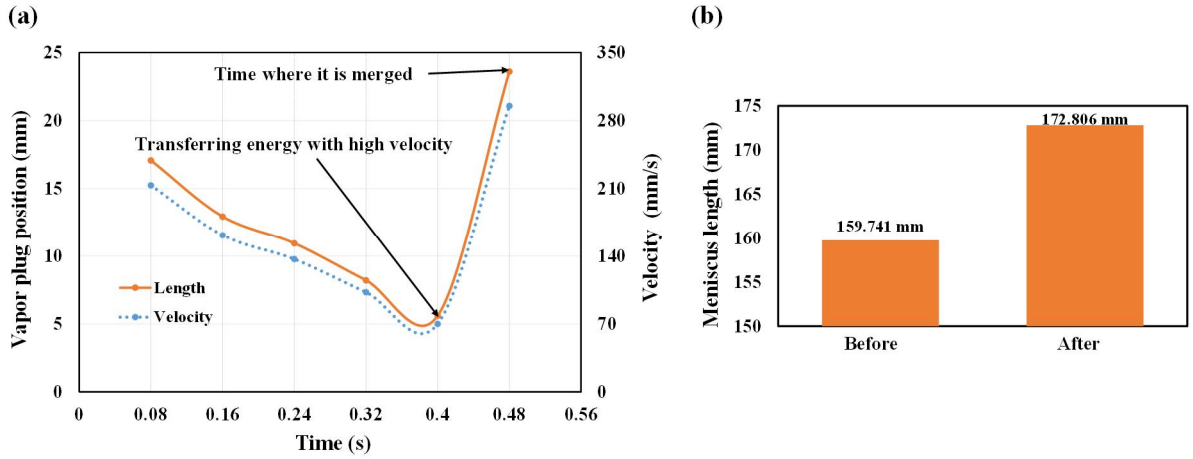

Fig 3.21. (a) Energy-transfer phenomena for a single VP, along with the velocity at Q = 35 W. (b) Meniscus length before (left) and after (right) VP merging.

With the Q_{in} of 35 W, other interesting flow phenomena were observed. When an annular and semi-annular flow rose from the evaporator section to the condenser section, one of the channels was fully wetted by the thin film, and multiple flow patterns were observed in other channels simultaneously. Fig. 3.22 shows the phenomena with the liquid film wetting the entire

channel with a large VP, which tended to increase its amplitude in its own position with a higher velocity. Channel I consisted of the liquid film marked with a rectangular shape, which wetted the entire section in a downward position after a duration of 0.40 ms. In channel II, a large AVP moved to the condenser section, as marked with a red arrow in Fig. 3.22. In channel III, there was a large VP (referred to as VP3). The behavior of VP3 is presented in Fig. 3.23. The oscillation amplitude of VP3 broadened, and its velocity increased. At this stage, both larger-amplitude oscillations and an arbitrary circulation led to higher thermal performance, as well as a far more stable flow regime. The heat-transfer rate was significantly higher, owing to the combination of latent and sensible heat transfer caused by the wetted liquid thin film, which was repulsed back to the condenser section with a high pressure [28].

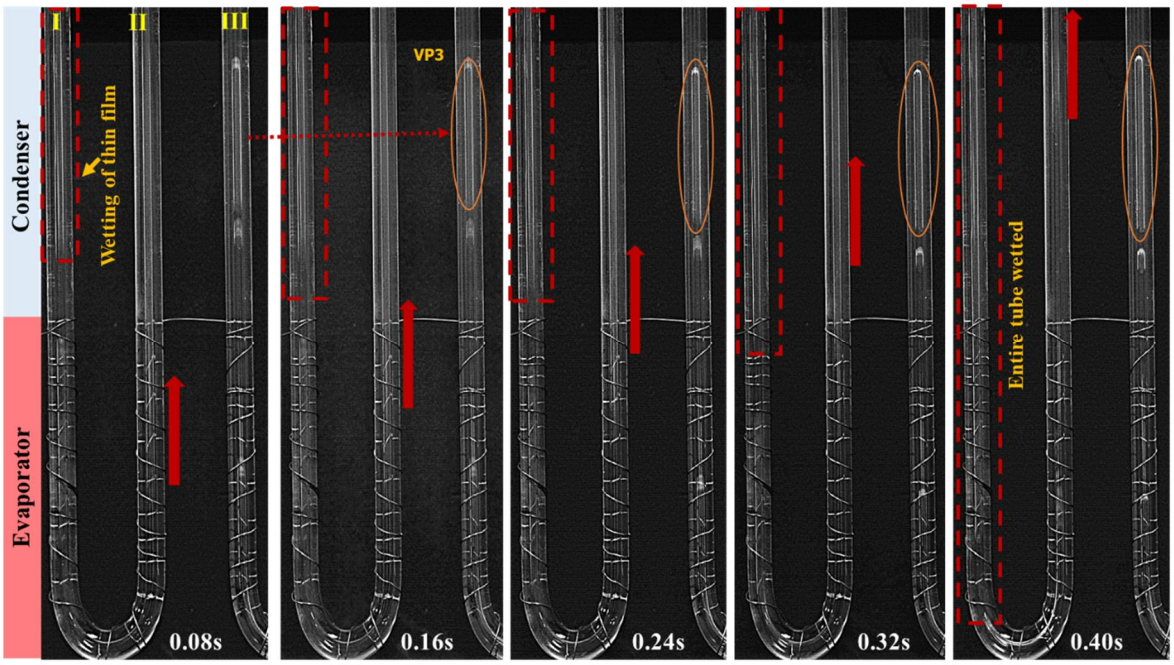

Fig 3.22. Thin-film evaporation and elongation of the VP (VP3) in the consecutive channels, along with oscillations of the AVP with respect to time.

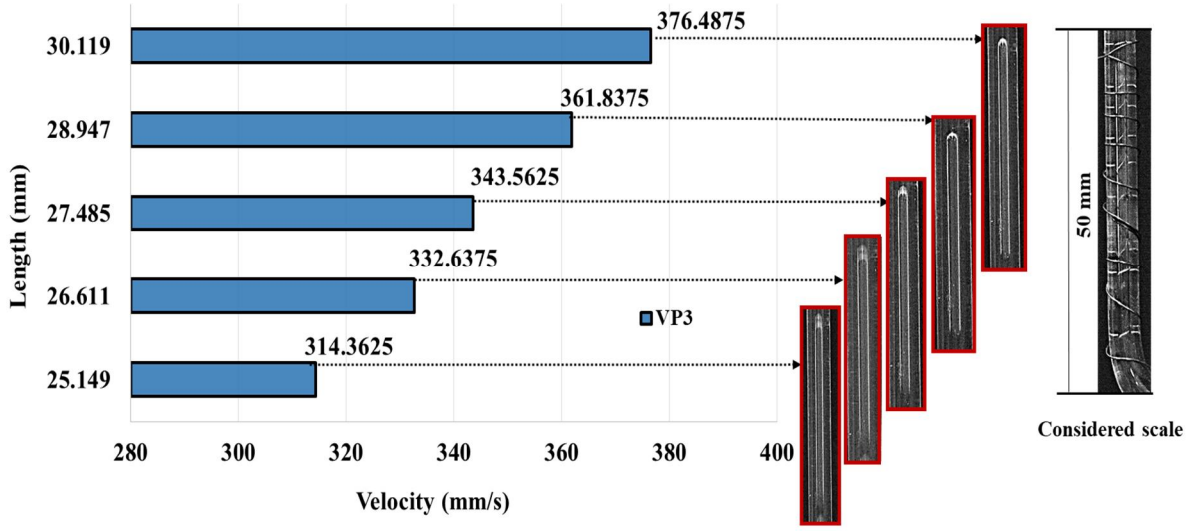

Fig 3.23. Position of VP (VP3) elongation in the channel at Q = 35 W, with respect to the velocity.

In the end process for the 35-W Q_{in}, the larger AVPs having upper-comer and down-comer meniscus heads were detected. Fig. 3.24(a) presents the visual status of the AVPs oscillating with a larger amplitude and adjoined in the U-shaped section. Fig. 3.24(b) presents the position of the meniscus heads with respect to time, where the blue bar indicates the meniscus position in channel I and the orange bar indicates the meniscus position in channel II. Initially, this oscillation started with a perfectly U-shaped AVP. Compared with the change of the meniscus position entering the evaporation section in channel I, that moving in an upward direction in channel II was large. This indicates that the increase in the overall length of the AVP increased the heat-transfer amount. There was one small vapor bubble in channel I, which was condensed and proceeded toward the AVP which merges with other bubbles later on.

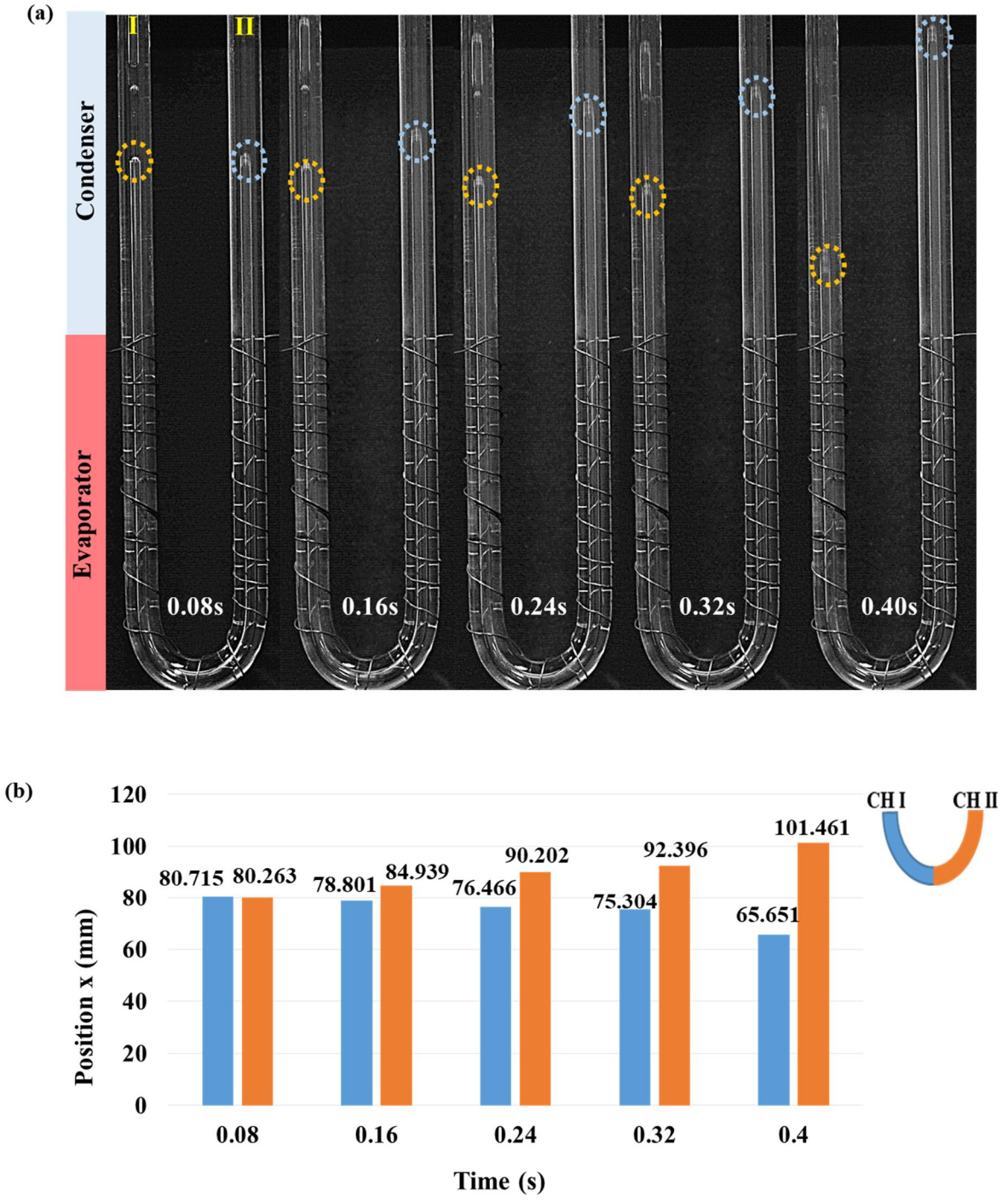

Fig 3.24. (a) Appearance of the larger AVP with the semi-annular flow in the down comer and the annular flow in the upper comer at Q_{in} = 35 W. (b) Positions of the upper comer and down comer with respect to time.

Fig. 3.25 presents a comparison of oscillation amplitudes with a Q_{in} difference of 5 W. The observations were taken for the oscillating motion of the VP in channel 1R. At the Q_{in} of 35

W in Fig. 3.25(a), the oscillation amplitude was on the order of 19.24 mm when the flows moved upward to the condenser section. When the flows moved downward to the evaporator section, the amplitude of the oscillations decreased and was in the range of 8.84 mm. In contrast, with the increasing Q_{in}, the amplitudes exceeded 30 mm, and the downward flows had a larger amplitude (56.46 mm at Q_{in} = 40 W) than the upward flows (33.00 mm at Q_{in} = 40 W). Thus, after the moderate heat load (30 W), a small increase in Q_{in} led to a significant change in the oscillations for the FR of 50%.

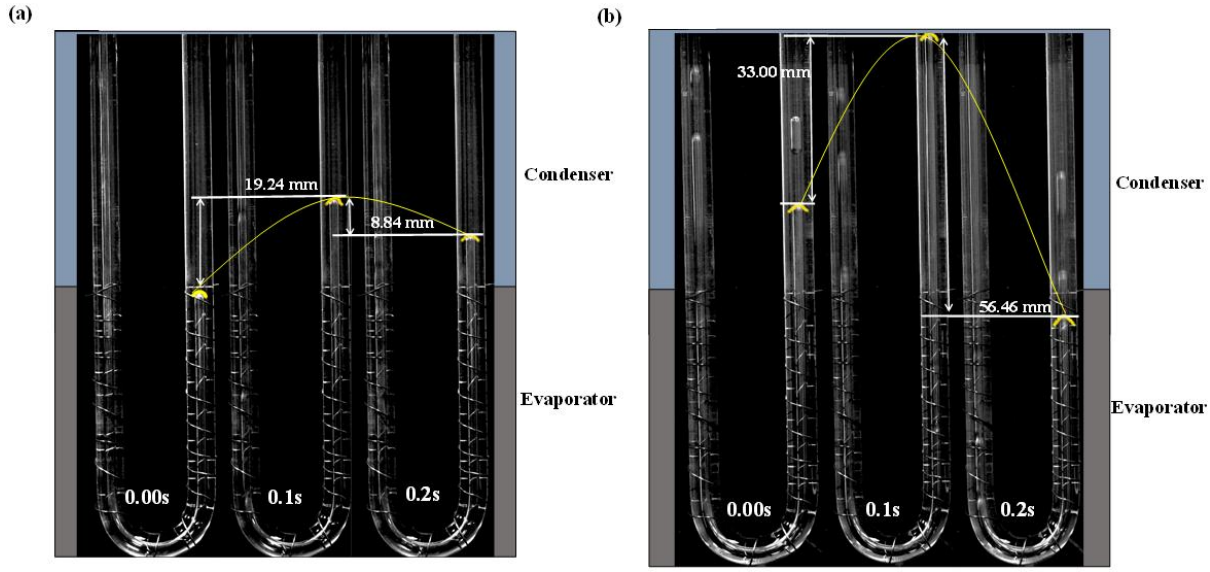

Fig 3.25. Comparison of the oscillation amplitudes for the 50% FR at Q_{in} values of (a) 35 W and (b) 40 W.

Fig. 3.26(a) presents snapshots of the meniscus motions in the evaporator and condenser sections in channels I and II. In the initial state, there were only two large VPs and two LSs. However, these LSs were divided by very small VPs, leading to a total of four VPs, including two large VPs and four LSs. Fig. 3.26(b) shows the oscillating motions of the meniscus with respect to time inside the capillary channels. The VP was connected through a U-channel in the evaporator section, where these menisci oscillated in perfect harmonic motions with large

amplitudes. The amplitude of the meniscus was calculated using the time-averaged location of the meniscus head. The time-averaged positions of the meniscus are shown in Fig. 3.26(c). The menisci oscillated for a very short time in the evaporator region and had smaller amplitude positions as well. They oscillated with higher amplitudes in the condenser section, for longer periods. Fig. 3.26(c) also reveals that as the meniscus head reached the evaporator section, it did not linger and carried the heat added to the condenser section in a very short time. Therefore, the majority of the meniscus head locations and oscillations were observed in the condenser section.

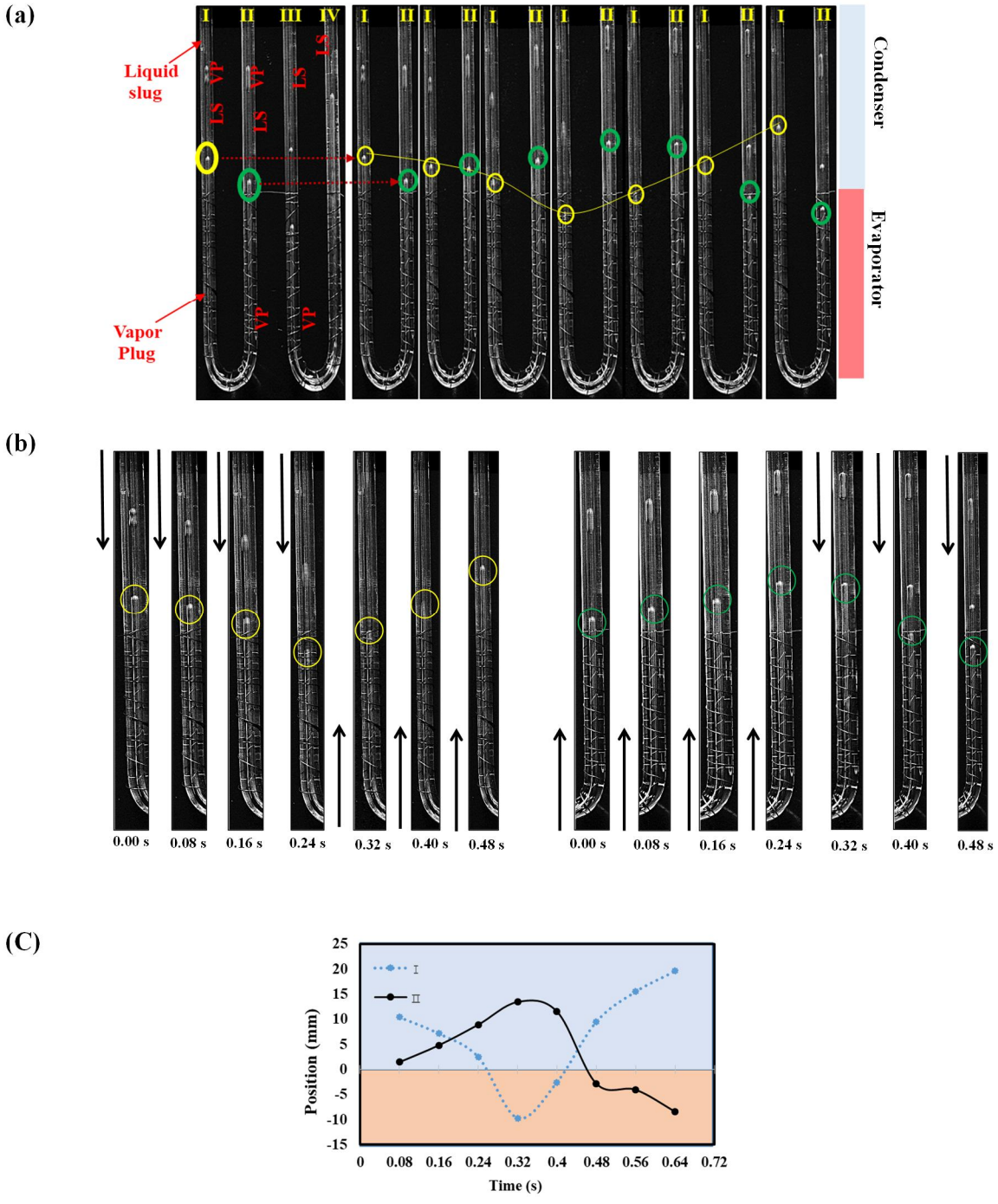

Fig 3.26. Meniscus locations in the evaporator and condenser sections. (a) Snapshots of the menisci locations, (b) expanded view with respect to time and the directions of motions, and (c) positions of the menisci.

4. Conclusion

The primary aim of this study was to understand the thermo-hydrodynamic of these two-phase heat transfer devices with checking its limits in different convection sources, two different experimental set-ups have been envisioned, fabricated, and tested in a laboratory. The set-up is specially designed for flow visualization, which can better define the flow regime trends when the heat load is increased. The primary influence parameter which affects the thermo-fluidic properties of the systems are as follows;

- Convection source and length
- Volumetric filling ratio
- Fill ratio consistent with convection source
- Orientation
- Thermo-physical properties
- Heat flux

The thesis provides a detailed discussion on the performance of CLPHP when subjected to different convection sources under vertical bottom heating mode orientation, especially the limits were checked the convection sources in the first experiment. The optimal filling ratio was found out when the ambient conditioned cooled the system in another experiment. For two different experiments, two different working fluid is used, hence the performance has been checked with different thermo-physical properties. Of course, the flow regimes were captured for both of the experiments to understand the bubble dynamics with different convection sources and working fluid. Apart from the working fluid and heat flux, the performance is strongly linked with the flow patterns existing inside the device. Delicate aspects of these two-phase flow dynamics and their relations with the heat transfer characteristics have been emphasized leading to the formulation of primary design rules. The

present studies can be used as a scale for future innovative industrial applications based on its thermo-hydrodynamics properties.

Although some nuances of the device operation remain unexplored, it is believed that major advancement in the understanding of the thermo-hydrodynamics of CLPHPs for different convection sources, and the optimal filling ratio for natural convection has been accomplished.

An innovative GT-CLPHP device with two turns was constructed to study the thermo-hydrodynamics behavior of CLPHP. Two sets of experiments are performed, one of which is the comparison between free and forced convection using methanol as a working fluid, and another study is to find out the optimal FR of ethanol as a working fluid and its flow regimes under ambient environmental conditions. For various values of Q_{in} and FR, R_{th} was derived from the temperature data, and flow patterns were captured using a high-speed camera. The main findings from the experimental study are as follows:

- The heat transfer characteristics and flow behavior depend largely on the source of convection, which also characterizes the operating range of the CLPHP from start-up to dry-out conditions. When the condenser section was exposed to natural convection, the performance period was very short. Whereas the performance duration was higher for the forced convection source when methanol is employed as a working fluid
- For low Q_{in}, the free convective CLPHP is effective. In contrast, for high Q_{in}, the forced convective CLPHP is effective.
- The initial start-up pulsation for the free convective operation was observed at a Q_{in} value of 24 W, while the start-up pulsation during forced convection CLPHP was observed at the Q_{in} of 18 W. Which indicates that the forced convection is effective

for early pulsations when 50% FR methanol is employed.

- The uni-directional slug/plug flow and oscillatory annular flow were dominant for free convective CLPHP at low Q_{in} and high Q_{in}, respectively. Initial dry-out was observed at a Q_{in} of 50 W for the free convective during the working fluid methanol.
- Uni-directional slug-plug flow, elongated plug flow, transition flow with liquid ring and liquid bridge, and oscillatory annular flow with large amplitudes along with LTF were observed for the forced convective CLPHP for Q_{in} values ranging from 18 W to 80 W. The initial dry-out occurs at the Q_{in} value of 80 W for forced convection.
- The bubble displacement was irregular-marginal for the free-convective CLPHP operation because its large section was exposed to ambient conditions, thereby allowing bubbles to oscillate with higher velocity (mean average velocities 0.001 m/s to 1.5 m/s), increasing T_c, and hence, decreasing R_{th}.
- Oscillations are observed to be regular, starting from a small amplitude to a large amplitude concerning Q_{in} for forced convective CLPHP. The average oscillation velocities are within the range of 0.075 m/s to 0.49 m/s.
- Acceleration of the bubbles increases with an increase in Q_{in} for both free and forced convective operations. The mean acceleration for the forced convective CLPHP is higher than that for the free convective CLPHP.
- The ambient conditions were sufficient to create a specific restoring force for condensation; hence, the device can be used in the open environment by maintaining a temperature conducive to sufficient condensation (25 ± 5 ℃). The optimal FR for the present study was found to be 50% FR according to the R_{th} results, and the lowest R_{th} was 1.67 ℃/W (at a Q_{in} of 40 W) using ethanol as a working fluid.

- According to the flow-visualization studies, at a low Q_{in} for the 50% FR, the flow patterns were mostly LSs and VPs, causing unstable thermal performance. However, as Q_{in} increase*d*, the flow pattern changed and took the shape of larger VPs and AVPs, particularly for Q_{in} > 25 W when ethanol is employed as a working fluid.
- A fascinating flow, i.e., the liquid thin film wrapping the VP, was observed. A liquid element film wetting the entire channel was also observed. These flows enhanced the thermal performance by increasing the heat-transfer coefficient. Such patterns were mostly observed at Q_{in} values of 30 and 35 W. Compared with the evaporation-section oscillations of the VP, the menisci had higher amplitudes and longer durations in the condenser section.

The present study concludes that the free convective CLPHP will be effective to transfer heat for a low Q_{in}. Whereas, the forced convective CLPHP can be effective to use for a longer duration of the operation and high Q_{in} based on its dry-out conditions. Besides the investigation can be useful in improving an understanding of the complex thermo-hydrodynamic phenomena of CLPHP when a different cooling source is provided for condensation. Even though the system has a very simple geometry (two-turns), this study can provide a benchmark for the numerical modeling of CLPHP when a higher number of turns are used for practical applications. Similarly, the study can be helpful to design a CLPHP system that operates under ambient conditions, with straightforward, ecofriendly, and efficient performance when using 50 % FR ethanol as a working fluid. The CLPHP that operates under ambient conditions will be also a valuable addition to the Solar-energy collection by using nano-particles or hybrid nano-fluids.

5. Remarks

The study presented in this thesis is the experimental approach to understand the thermo-hydrodynamics of CLPHP when subjected to different convection sources. Also, the performance has been checked for ambient cooling conditions, which will be valuable for storing the new-energy in the form of solar, besides the electronics and space technologies. While many of the aspects have been covered in this study, it will indeed be very naive to extend the research to the present research scope. The future study should be directed towards the making of technology of PHP to become more standard for industrial applications. Based on the expertise in the current study the following suggestions may prove to be helpful in this direction.

- Of course, these two-phase passive heat-transfer devices are very helpful in the cooling of electronics and space technology, the research can be further extended to design a CLPHP with more number of turns in the ambient conditions for the energy collection, where this device can work as a Heat exchanger. (Using nano-fluids for solar energy collection through these heat pipes will be the best option for the solar intensity.
- Various working fluids had shown its better performance in these heat pipes, however, its hydrodynamic study is not yet fully understood. A detailed study on the working fluid selection based on ith Thermo-hydrodynamic can be a greater addition to the research on the PHPs.
- The dry-out mechanism certainly remained unexplored, depending on the materials and working fluid, which is needed to understand for future research technology.
- Apart from the numerical study on the velocity information of the bubble or

flow phase, there are very few studies and had been neglected by many researchers. Considering the velocity information on the flow regimes can play a vital role to understand the physics behind the thermally driven flow regime.

- At last, a comprehensive scheme for the mathematical modeling of these devices are also neglected and should be considered for better understanding.

REFERENCE

[1] F. P. H. Akachi, P. Stulc, "Pulsating heat pipes," *Proceedings of the 5th International Heat Pipe Symposium*, pp. 208–217, 1996.

[2] Han, X.H., Wang, X.H., Zheng, H.C., Xu, X.G., and Chen, G.M., *Review of the development of pulsating heat pipe for heat dissipation.* Renew Sust Energ Rev, 2016. **59**: 692-709.

[3] Nazari, M.A., Ahmadi, M.H., Ghasempour, R., Shafii, M.B., Mahian, O., Kalogirou, S., and Wongwises, S., *A review on pulsating heat pipes: From solar to cryogenic applications.* Appl Energ, 2018. **222**: 475-484.

[4] Yang, H., Khandekar, S., and Groll, M., *Performance characteristics of pulsating heat pipes as integral thermal spreaders.* Int J Therm Sci, 2009. **48**(4): 815-824.

[5] Abad, H.K.S., Ghiasi, M., Mamouri, S.J., and Shafii, M.B., *A novel integrated solar desalination system with a pulsating heat pipe.* Desalination, 2013. **311**: 206-210.

[6] Khandekar, S., Charoensawan, P., Groll, M., and Terdtoon, P., *Closed loop pulsating heat pipes Part B: visualization and semi-empirical modeling.* Appl Therm Eng, 2003. **23**(16): 2021-2033.

[7] Liu, S., Li, J.T., Dong, X.Y., and Chen, H.Z., *Experimental study of flow patterns and improved configurations for pulsating heat pipes.* J Therm Sci, 2007. **16**(1): 56-62.

[8] Ning Qian, Yucan Fu, Yuwen Zhang, Jiajia Chen, Jiuhua Xu, Experimental investigation of thermal performance of the oscillating heat pipe for the grinding wheel, International Journal of Heat and Mass Transfer,Volume 136,2019,

[9] Khandekar, S., Dollinger, N., and Groll, M., *Understanding operational regimes of closed loop pulsating heat pipes: an experimental study.* Appl Therm Eng, 2003. **23**(6): 707-719.

[10] Charoensawan, P., Khandekar, S., Groll, M., and Terdtoon, P., *Closed loop pulsating heat pipes: Part A: parametric experimental investigations.* Appl Therm Eng, 2003. **23**(16): 2009-2020.

[11] Yang, H.H., Khandekar, S., and Groll, M., *Operational limit of closed loop pulsating heat pipes.* Appl Therm Eng, 2008. **28**(1): 49-59.

[12] Ayel, V., Araneo, L., Scalambra, A., Mameli, M., Romestant, C., Piteau, A., Marengo, M., Filippeschi, S., and Bertin, Y., *Experimental study of a closed loop flat plate pulsating heat pipe under a varying gravity force.* Int J Therm Sci, 2015. **96**: 23-34.

[13] S. S. Bhakre, Choudhari, Md. Rafik Sajjadahmad, "Experimental Analysis on Effect of Design Parameters on the Performance of Single Loop Pulsating Heat Pipe," *Conference Proceedings*, 2015.

[14] H. R. Goshayeshi, M. Goodarzi, M. R. Safaei, "Experimental study on the effect of inclination angle on heat transfer enhancement of a ferrofluid in a closed loop oscillating heat pipe under magnetic field," *Experimental Thermal and Fluid Science,* vol. 74, pp. 265-270, 2016/06/01/, 2016.

[15] C. B. R. Kothare, Kinshuk Chavhan, Balu K., "Thermal performnace of closed loop pulsating heat pipes at various dimensions and heat input," *Conference Proceedings*, 2015.

[16] Z. Xue, and W. Qu, "Experimental study on effect of inclination angles to ammonia pulsating heat pipe," *Chinese Journal of Aeronautics,* vol. 27, no. 5, pp. 1122-1127, 2014/10/01/, 2014.

[17] H. Yang, S. Khandekar, and M. Groll, "Operational limit of closed loop pulsating heat pipes," *Applied Thermal Engineering,* vol. 28, no. 1, pp. 49-59, 2008/01/01/, 2008.

[18] M. Alhuyi Nazari, M. H. Ahmadi, R. Ghasempour, "How to improve the thermal performance of pulsating heat pipes: A review on working fluid," *Renewable and Sustainable Energy Reviews,* vol. 91, pp. 630-638, 2018/08/01/, 2018.

[19] D. S. Jang, H. J. Chung, Y. Jeon, "Thermal performance characteristics of a pulsating heat pipe at various nonuniform heating conditions," *International Journal of Heat and Mass Transfer,* vol. 126, pp. 855-863, 2018/11/01/, 2018.

[20] W. Jiansheng, W. Zhenchuan, and L. Meijun, "Thermal performance of pulsating heat pipes with different heating patterns," *Applied Thermal Engineering,* vol. 64, no. 1, pp. 209-212, 2014/03/01/, 2014.

[21] M. Saha, Feroz, C.M., Ahmed, F, "Thermal performance of an open loop closed end pulsating heat pipe," *Heat Mass Transfer* vol. 48, pp. 259, 2012.

[22] R. Zamani, Kalan, K. & Shafii, M.B. , "Experimental investigation on thermal performance of closed loop pulsating heat pipes with soluble and insoluble binary working fluids and a proposed correlation," *Heat Mass Transfer,* vol. 55, pp. 375, 2019.

[23] S. Khandekar, A. P. Gautam, and P. K. Sharma, "Multiple quasi-steady states in a closed loop pulsating heat pipe," *International Journal of Thermal Sciences,* vol. 48, no. 3, pp. 535-546, 2009/03/01/, 2009.

[24] S. Lips, A. Bensalem, Y. Bertin, "Experimental evidences of distinct heat transfer regimes in pulsating heat pipes (PHP)," *Applied Thermal Engineering,* vol. 30, no. 8, pp. 900-907, 2010/06/01/, 2010.

[25] M. Mameli, M. Marengo, and S. Khandekar, "Local heat transfer measurement and thermo-fluid characterization of a pulsating heat pipe," *International Journal of Thermal Sciences,* vol. 75, pp. 140-152, 2014/01/01/, 2014.

[26] B. Y. Tong, T. N. Wong, and K. T. Ooi, "Closed-loop pulsating heat pipe," *Applied Thermal Engineering,* vol. 21, no. 18, pp. 1845-1862, 2001/12/01/, 2001.

[27] J. L. Xu, Y. X. Li, and T. N. Wong, "High speed flow visualization of a closed loop pulsating heat pipe," *International Journal of Heat and Mass Transfer,* vol. 48, no. 16, pp. 3338-3351, 2005/07/01/, 2005.

[28] D. Mangini, M. Marengo, L. Araneo, "Infrared analysis of the two phase flow in a single closed loop pulsating heat pipe," *Experimental Thermal and Fluid Science,* vol. 97, pp. 304-312, 2018/10/01/, 2018.

[29] K.-S. Yang, Y.-C. Cheng, M.-C. Liu, "Micro pulsating heat pipes with alternate microchannel widths," *Applied Thermal Engineering,* vol. 83, pp. 131-138, 2015/05/25/, 2015.

[30] A. Yoon, and S. J. Kim, "Characteristics of oscillating flow in a micro pulsating heat pipe: Fundamental-mode oscillation," *International Journal of Heat and Mass Transfer,* vol. 109, pp. 242-253, 2017/06/01/, 2017.

[31] A. Yoon, and S. J. Kim, "Experimental and theoretical studies on oscillation frequencies of liquid slugs in micro pulsating heat pipes," *Energy Conversion and Management,* vol. 181, pp. 48-58, 2019/02/01/, 2019.

[32] T. N. Mito, Kyohei Yanagi, Nagato Tamura, Hitoshi Terazaki, Yoshiro, "Enhancement of Thermal Properties of HTS Magnets Using Built-in Cryogenic Oscillating Heat Pipes," *IEEE Transactions on Applied Superconductivity,* vol. V 23, pp. 4602905-4602905, 2013.

[33] T. Mito, K. Natsume, N. Yanagi, "Achievement of High Heat Removal Characteristics of Superconducting Magnets With Imbedded Oscillating Heat Pipes," *IEEE Transactions on Applied Superconductivity,* vol. 21, no. 3, pp. 2470-2473, 2011.

[34] F. Bonnet, P. Gully, and V. Nikolayev, "Development and test of a cryogenic pulsating heat pipe and a pre-cooling system," *AIP Conference Proceedings,* vol. 1434, no. 1, pp. 607-614, 2012/06/12, 2012.

[35] H. R. Deng, Y. M. Liu, R. F. Ma, "Experimental investigation on a pulsating heat pipe with hydrogen," *IOP Conference Series Materials Science and Engineering (Online),* vol. 101, no. 1, pp. 8, 2015.

[36] L. D. Fonseca, F. Miller, and J. Pfotenhauer, "Design and Operation of a Cryogenic Nitrogen Pulsating Heat Pipe," *IOP Conference Series: Materials Science and Engineering,* vol. 101, pp. 012064, 2015/12/18, 2015.

[37] L. D. Fonseca, F. Miller, and J. Pfotenhauer, "Experimental heat transfer analysis of a cryogenic nitrogen pulsating heat Pipe at various liquid fill ratios," *Applied Thermal Engineering,* vol. 130, pp. 343-353, 2018/02/05/, 2018.

[38] D. Xu, L. Li, and H. Liu, "Experimental investigation on the thermal performance of helium based cryogenic pulsating heat pipe," *Experimental Thermal and Fluid Science,* vol. 70, pp. 61-68, 2016/01/01/, 2016.

[39] L. D. Fonseca, J. Pfotenhauer, and F. Miller, "Short communication: Thermal performance of a cryogenic helium pulsating heat pipe with three evaporator sections," *International Journal of Heat and Mass Transfer,* vol. 123, pp. 655-656, 2018/08/01/, 2018.

[40] L. D. Fonseca, F. Miller, and J. Pfotenhauer, "A helium based pulsating heat pipe for superconducting magnets," *AIP Conference Proceedings,* vol. 1573, no. 1, pp. 28-35, 2014/01/29, 2014.

[41] X. Cui, Z. Qiu, J. Weng, "Heat transfer performance of closed loop pulsating heat pipes with methanol-based binary mixtures," *Experimental Thermal and Fluid Science,* vol. 76, pp. 253-263, 2016/09/01/, 2016.

[42] S. Khandekar, P. Charoensawan, M. Groll, "Closed loop pulsating heat pipes - Part B: Visualization and semi-empirical modeling," *Applied Thermal Engineering,* vol. 23, pp. 2021-2033, 11/01, 2003.

[43] H. Ma, M. A. Hanlon, and C.-l. Chen, "An investigation of oscillating motions in a miniature pulsating heat pipe," *Microfluidics and Nanofluidics,* vol. 2, pp. 171-179, 03/01, 2006.

[44] S. Okazaki, H. Fuke, H. Ogawa, "Development of Meter-scale O-shaped and U-shaped Oscillating Heat Pipes for GAPS." pp. 1-9.

[45] V. M. Patel, Gaurav, and H. B. Mehta, "Influence of working fluids on startup mechanism and thermal performance of a closed loop pulsating heat pipe," *Applied Thermal Engineering,* vol. 110, pp. 1568-1577, 2017/01/05/, 2017.

[46] K. R. V. K. Karthikeyan, B. C. Pillai., "Understanding thermo-fluidic characteristics of a glass tube closed loop pulsating heat pipe: flow patterns and fluid oscillations," *Heat Mass Transfer,* vol. 51, no. 12, pp. 1669–1680, December 2015, 2015.

[47] N. Iwata, H. Ogawa, and Y. Miyazaki, "Maximum Heat Transfer and Operating Temperature of Oscillating Heat Pipe," *Journal of Heat Transfer,* vol. 138, no. 12, pp. 122002-122002-5, 2016.

[48] Khandekar, S., and Groll, M. *Insights into the Performance Modes of Closed Loop and Pulsating Heat Pipes and Some Design Hints*. in *Proceedings of the 18th National & 7th ISHMT-ASME Heat and Mass Transfer Conference*. 2006. Guwahti, India

[49]. Betancur, L., Mangini, D., Mameli, M., Filippeschi, S., Kessler Slongo, L., Paiva, K., Mantelli, M., and Marengo, M., *Condenser Temperature Effect on the Transient Behavior of a Pulsating Heat Pipe.* 2016.

[50] Spinato, G., Borhani, N., and Thome, J.R., *Understanding the self-sustained oscillating two-phase flow motion in a closed loop pulsating heat pipe.* Energy, 2015. **90**: 889-899.

[51] Pachghare, P.R. and Mahalle, A.M., *Thermo-hydrodynamics of closed loop pulsating heat pipe: an experimental study.* J Mech Sci Technol, 2014. **28**(8): 3387-3394.

[52] Bar-cohen, Trends in packaging of computer systems, in cooling of electronic systems, edited by kakac S., Yuncu H. and Hijikata, Kulwar academic publishers, pp. 17-45, 1994.

[53] Vasiliev, L.L, 2002, "Heat Pipe Thermal Control for Sorption Machines," Proceedings of 12th International Heat Pipe Conference, Moscow, Russia, pp.65- 73.

[54] Shafii, M.B., Faghri Amir and Zhang Yuwen, December 2001, "Thermal Modeling of Unlooped and Looped Pulsating Heat Pipes," Journal of Heat Transfer, Vol. 123,pp. 1159-1172.

[55] Liang, S.B. and Ma, H.B., 2004, "Oscillating Motions of Slug Flow in Capillary Tubes," International C 3, pp.365-375

[56] Nishio, S., 2004, "Single-Phase Laminar-Flow Heat Transfer and Two-Phase Oscilating Flow Heat Transport in Microchannels," Heat Transfer Engineering, Vol. 25, No. 3, pp.31-43.

[57] Kammuang-Lue, N., Sakulchangsatjatai, P., Terdtoon, P., and Mook, D.J., *Correlation to Predict the Maximum Heat Flux of a Vertical Closed-Loop Pulsating Heat Pipe.* Heat Transfer Eng, 2009. **30**(12): 961-972.

Acknowledgment

I would like to express my sincere gratitude to my advisor, Professor Sung Yong Jung for guiding and supporting me over these 2 years. The journey would have been impossible has I not received your guidance. You have been much more to me than all the meanings and interpretations this word can embody. Your personality has left an unprecedented impression on me and I am not able enough to thank you by words. You have an example of excellence as a researcher, mentor, and role model. Also, I would like to thank all the professors of Thermal division of the Department of Mechanical Engineering, all of their guidance through this process; your discussion, ideas, and feedback have been absolutely invaluable.

I would like to express my appreciation and thanks to all of the FVL members, guys you have been tremendous colleagues for me. Your advice and help on both research and Korean culture have been priceless.